The Thesis Committee for Nanzhu Zhao
Certifies that this is the approved version of the following thesis:

An Electrical Resistance-based Fatigue Life Prediction Model and Its Application in Lithium-Ion Battery Ultrasonic Welding

APPROVED BY
SUPERVISING COMMITTEE:

Supervisor:

Wei Li

Dragan Djurdjanovic

An Electrical Resistance-based Fatigue Life Prediction Model and Its Application in Lithium-Ion Battery Ultrasonic Welding

by

Nanzhu Zhao, B.S.

Thesis

Presented to the Faculty of the Graduate School of

The University of Texas at Austin

in Partial Fulfillment

of the Requirements

for the Degree of

Master of Science in Engineering

The University of Texas at Austin

December 2012

Dedication

To my father who has been the guiding light in my life and to my mother for all the joy and love she brought to my life.

Acknowledgements

I would like to thank my parents for their consistent support and encouragement throughout my college life. I am sincerely grateful for all their sacrifices for me.

I would also like to thank my research advisor Dr. Wei Li whose guidance, inspiration and support made it possible for me to start this research project and eventually be able to complete this thesis. I would like to thank Dr. Wayne Cai for his effort and advice on the project. I am also thankful to Bryan Philpott who has been helping me throughout the project. I would like to thank Dr. Djurdjanovic for serving on my thesis committee.

Last, but not least, I would like to acknowledge Dr. Akella, Dr. Longoria and Dr. Chen for their inspirational teaching in the area of Dynamic Systems and Controls. I would have never been able to gain so much experience without their challenging and insightful courses.

December 2012

Abstract

An Electrical Resistance-based Fatigue Life Prediction Model and Its Application in Lithium-Ion Battery Ultrasonic Welding

Nanzhu Zhao, M.S.E.

The University of Texas at Austin

2012

Supervisor: Wei Li

Ultrasonic welding is one of the leading technologies for joining multiple, thin sheets of dissimilar materials, such as copper and aluminum, for automotive lithium-ion batteries. The performance of ultrasonic welds, particularly the fatigue life, however, has not been well studied. In this work, a theoretical fatigue life model for ultrasonically welded joints was developed using continuum damage mechanics. In the model, the damage variable was defined as a function of the increase of the joint electrical resistance, resulting in an electrical resistance-based fatigue life prediction model. The fatigue model contains two constants to be determined with experimental data, depending on different fatigue loads and joint properties. As an application, the fatigue life model was validated for Al-Cu lithium-ion battery tab joints. Mechanical fatigue tests were

performed under various stress loading conditions for welds made using different welding parameters. It is shown that the developed model can be used to predict the remaining life of the ultrasonically welded battery tab joints for electric and hybrid electric vehicles by monitoring the electrical resistance change.

In addition, thermal and electrical fatigue tests were performed for Al-Cu battery tab welds using simulated operating conditions of electrical vehicles. These included temperature cycling between -40 and 90 °C and current cycling of 0 to 10 A. All the tests were conducted on individual weld joints. The results showed that the thermal and electrical loads imposed insignificant effect on the electrical resistance of the battery tab joints.

Table of Contents

List of Tables

List of Figures

Chapter 1: Introduction

1.1 Lithium-ion Batteries in Vehicles

Lack of fossil fuel supply, air pollution, and global warming due to greenhouse gas emission are all major environmental issues under exploration nowadays. Fossil fuels such as petroleum and coal are limited in supply and will eventually be depleted. In addition, excessive consumption of these fuels for transportation will lead to severe air pollution in urban areas and thus result in negative health effects on human beings. In the United States, 68% of oil consumption and 36–78% of ingredients causing air pollution are generated by the transportation sector. Also, 28% of greenhouse gas emission and 34% of CO_2 emission are from the transportation sector [1]. Therefore, finding an alternative to the conventional vehicle powered by an internal combustion engine is critical for reducing the overall fuel consumption as well as decreasing air pollution and greenhouse gas emission. Consequently, an ever-increasing demand for a clean and sustainable source of energy has spurred automotive industry to produce more electric vehicles. Since the first mass production of the EV1 by General Motors in 1996, battery powered vehicles have provided a green and renewable energy transition from traditional combustion engines to electric motors. Due to the high power and energy density, Lithium-ion batteries has become the major power source of EV (Electric Vehicle), HEV (Hybrid Electric Vehicle) and PHEV (Plug-in Hybrid Electric Vehicle) [2, 3].

In general, EV refers to the vehicle that uses batteries as the primary energy source in the powertrain system with an electric motor and thus has a great potential to

eliminate its dependency on gasoline. A HEV commonly uses both an internal combustion engine and an electric motor to produce higher fuel economy by recycling the energy loss due to braking and excess engine operation. Then the excessive energy is stored in the battery pack, which will be used to propel the vehicle [4]. The major difference between a PHEV and a HEV is that a PHEV can be plugged into an external power source to charge the battery. In addition, it can also be charged by a generator attached to the internal combustion engine or using regenerative braking [5]. The overall performance of all three types of vehicles relies on the quality and capacity of the battery packs. Therefore, the design and manufacturing of the lithium-ion battery packs for stable and reliable power supply is of great importance for their application in electric vehicles.

1.2 LITHIUM-ION BATTERY MANUFACTURING

In current automotive lithium-ion battery manufacturing, a battery pack is composed of several hundreds, or even more than a thousand battery cells based on the cell configuration and pack size in order to meet the power and energy requirement of the powertrain system in a vehicle [6]. A certain number of cells are joined together to form a unit; several units are connected with a common bus-bar to form a module; and then tens of modules are assembled into a battery pack. The battery tab joint is a critical component of the battery pack and can cause failure of the entire system if it breaks due to impact or fatigue. The electrical resistance of the battery tab joint is also important to the operation of an electric vehicle because the resistance increase could cause excessive energy loss due to joule heating [7]. Although lithium-ion battery systems have been successfully

used in many applications such as laptop computers, the harsh environment of automobiles imposes more stringent requirements on the battery joint performance including the fatigue life.

1.3 Electrical Resistance as An Indicator of Fatigue Life

The fatigue life of a metallic material is generally described by an S–N curve, also known as a Wöhler curve. When high amplitude stress is applied to the material that results in crack initiation, the crack growth rate can be related to the number of cycles directly by a power law function characterized by Coffin and Manson [8, 9]. Continuum damage mechanics allows for the prediction of fatigue life by measuring physical parameters that can represent the damage accumulation quantitatively, such as temperature, micro-hardness, toughness, energy dissipation, electrical potential drop, electrical resistance, and modulus degradation [10-14]. Among these methods, the electrical resistance measurement has received substantial attention due to its simple setup and nondestructive testing nature. In recent years, this method has been increasingly used to substitute mechanical strain measurements for high complexity materials and extensive cyclic loading conditions [15, 16]. Since the electrical resistance of a testing sample relies strongly on the microstructure and crack propagation of the material, the damage evolution in the sample yields a corresponding change of resistance in a characteristic manner [17, 18]. Same as material testing samples, the electrical resistance of an ultrasonic weld depends strongly on the geometric configuration and crack formation and progress of the welded area. Therefore, the electrical resistance

change over time or the number of loading cycles can be used for fatigue life evaluation. In addition, by monitoring the resistance change during the vehicle operation, it is possible to eventually predict the remaining life of the battery tab joint.

1.4 RESEARCH OBJECTIVES

The purpose of this research is to evaluate the feasibility of predicting the fatigue life of lithium-ion battery tab joints using electrical resistance. Specifically, the research objectives include:

- To develop a theoretical fatigue life model for ultrasonically welded joints based on electrical resistance measurements.
- To develop a method for fatigue life prediction using electrical resistance measurements.
- To conduct mechanical, thermal, and electrical fatigue tests in order to validate the developed model.

The fatigue model was developed based on continuum damage mechanics, where the damage variable was defined as a function of the increase of the joint electrical resistance. Mechanical fatigue tests were conducted under various stress loading conditions using welds made with different welding parameters. The mechanical fatigue test results were used to validate the developed model and the prediction method.

Chapter 2: Literature Review

2.1 Battery Pack Manufacturing

Automotive battery packing process can be divided into three levels, i.e., inside-cell joining, cell-to-cell joining, and unit-to-unit or module-to-module joining [6]. The hierarchy of battery pack manufacturing is shown in Fig. 2.1. As the smallest unit in a battery system, each battery cell is composed of a carbon anode, a metal oxide cathode and a lithium salt in an organic solvent electrolyte separated by cartridge in a rigid case. Two major joining processes are involved at the inside-cell level: joining of positive and negative electrodes and joining of electrodes to the battery tab. Due to very low thickness of the electrode films, the joining of these thin films requires a highly delicate welding process. Then, a certain number of these battery cells are joined together in series or in parallel to form a battery unit, which is the smallest battery unit that is replaceable without breaking any other units in the battery module. The joining at the unit level is composed of two parts: the joining of individual battery tab and the joining of battery tab to the bus bar. Compared with the cell level joining, multiple metallic layers need to be joined together at the unit level and the positive battery tab is made by aluminum while the negative tab is made by copper in general. This means that it also requires a dissimilar material joining process. More details on the component materials are presented in Table 2.1 [6]. Unit level joining is the most challenging process in battery pack manufacturing. The unit-to-unit and module-to-module joining can be commonly achieved by mechanical joining for ease of disassembly of battery packs.

In high level joining processes, due to the large volume of battery components, spatial efficiency will be the major concern while meeting the power consumption needs for vehicle operation. As mentioned above, a battery pack for electric vehicles is composed of hundreds of individual battery cells connected together to drive electric motors, which means there are a large number of joints connecting individual cells. Therefore, inappropriate joining at the cell-to-cell level or improper connection of a bolted joint with electrical lugs can cause excessive Joule heating, which will result in the breakdown of the joint between cells and eventually cause failure of the entire battery pack [19]. Consequently, designing of a robust and automated joining process is essential for mass production of the Lithium-ion battery packs in the automotive industry.

Aluminum, copper and nickel are the most commonly used battery tab materials due to the high electrical and thermal conductivity. However the weldability of these materials is the major challenge for mass production. Another obstacle that needs to be overcome is to join multiple layers of dissimilar materials with different sheet thickness combinations and various melting temperatures. In addition, relatively large weld areas are needed for lower electrical current density and higher mechanical strength. Furthermore, reliable joints are required for batteries to endure harsh environmental conditions such as extensive vibration, severe weather, high electrical current, and humidity

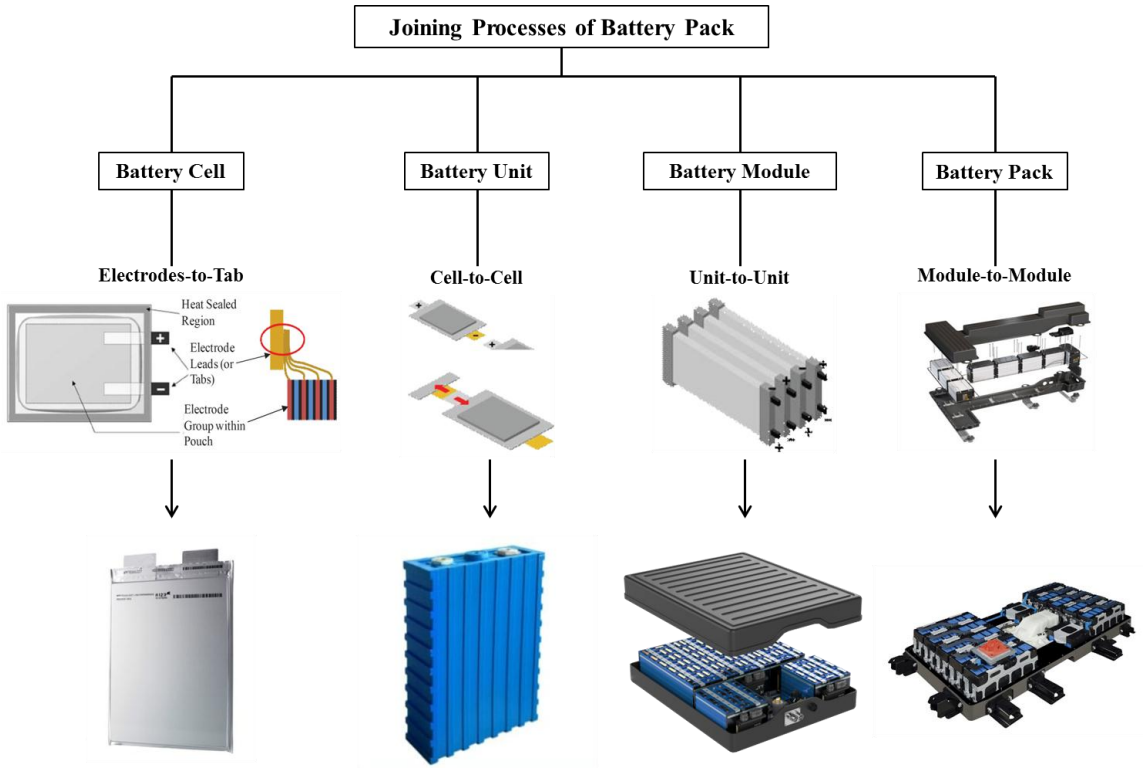

Figure 2.1 The hierarchy of battery pack manufacturing

Table 2.1 Component materials of lithium-ion batteries [6]

Battery Type	Cylindrical	Pouch Prismatic	Solid-container Prismatic
Anode Electrode	Copper	Copper	Copper
Negative Tab	Aluminum, Nickel	Copper	Aluminum, Nickel
Cathode Electrode	Aluminum	Aluminum	Aluminum
Positive Tab	Aluminum, Nickel	Aluminum	Aluminum, Nickel

2.2 JOINING TECHNOLOGIES IN BATTERY MANUFACTURING

Currently available joining technologies in battery manufacturing are reviewed and discussed in this section, which includes mechanical joining, electrical resistance welding, laser beam welding, and ultrasonic welding.

2.2.1 Mechanical Joining

There are various methods in mechanical joining used to fasten or clamp parts of an assembly. Fastening joints include nuts, screws, bolts, circlips, rivets, etc. Integral joining method includes seams, crimps, snap-fits, etc. Mechanical joints have been most commonly accepted for joining metals as well as plastic materials. In the battery pack manufacturing, due to battery maintenance and replacement concerns, mechanical joining is more appropriate for joining large modules using threaded bus bars or metal rods because of the ease of dismantling for maintenance and repair [6]. However, additional sealing materials are needed for mechanical joints in order to prevent corrosion by the passage of liquids and gases from the environment. Also, the threaded holes in a mechanical joint are the weakest spots and may cause failure by extensive vibration of the vehicles.

2.2.2 Electrical Resistance Welding

Electrical resistance welding includes a group of welding processes such as spot welding and seam welding that produce welds by a localized heat generated by the

electrical resistance at the interface of the materials when high current is passed through [20].

Electrical resistance welding has been widely accepted in electronics and automotive industries due to the high efficiency with automated production line and little pollution to the environment. In contrast, in the battery pack manufacturing, materials with high thermal and electrical conductivity such as aluminum, copper, and nickel are used as electrodes and tabs in lithium-ion batteries, which are difficult to be resistance welded. The weldability chart of battery tab materials is presented in Table 2.2. Additionally, electrical resistance welding is not suited for joining dissimilar materials due to different melting temperatures. Even through Various modifications of resistance welding such as projection welding and nickel plating on highly conductive materials have been introduced to battery tab welding, it still has major challenges to overcome, which includes poor weld quality for highly conductive metals, multi-layered materials and dissimilar materials.

Table 2.2 Weldability of battery tab materials in electrical resistance welding [6]

Materials	**Aluminum**	**Copper**	**Nickel**
Aluminum	Fair - electrode sticking	Difficult - low strength - electrode sticking	Difficult - low strength
Copper		Good	Fair - low strength
Nickel			Excellent

2.2.3 Laser Beam Welding

Laser beam welding is a welding process used to join multiple pieces of material by using a laser beam, which generates a concentrated heat at the interface, allowing for narrow and deep welds. Laser beam welding can produce a small heat affected area and join multiple sheets in a single process, which is ideal for volume production of weld joints. However, in battery pack manufacturing, most of the battery tab materials such as aluminum and copper are highly reflective and thermally conductive, which may result in poor quality in welding or even weld defects. Mechanical properties of the joints welded by the laser beam can be improved by modification of beam offset as well as a proper selection of the coating materials as the interlayer [21].

2.2.4 Ultrasonic Welding

Ultrasonic welding is one of the major joining methods currently used in the automotive industry for lithium-ion battery tab joints. The process generates oscillating shears by high power ultrasound to create solid-state joints between two or more layers of materials due to the propagation of the welds layer by layer as shown in Fig. 2.2. Compared with other joining methods, ultrasonic welding achieves better bonds between thin layers of dissimilar materials, especially those with high electrical and thermal conductivity such as copper and aluminum, which are essential for battery tab joints. Ultrasonic welding does not require any filler metal or gas, and can be performed at a low temperature. It can also be easily integrated with robots for automated operation. Moreover, ultrasonically welded joints can avoid typical metallurgical defects such as

formation of intermetallic compounds, brittle phases, and porosities in the fusion zone. However, the major disadvantage of ultrasonic welding is its limitation in the thickness of the layers as well as high variations of the weld quality resulted from welding conditions. On the other hand, battery tabs are typically made of thin layers of materials. Much research has been conducted to define the weld quality guidelines for ultrasonic welding, including the energy-based analytical model for metal foil deposition in ultrasonic consolidation using two factors: energy input within a cycle of ultrasonic motion and the total energy delivered. It was found that the linear weld density and the input energy were similarly influenced by oscillation amplitude, welding speed and clamping force [22, 23]. Therefore, with a proper control of the welding process, the characteristics of the solid-state joining method and the environmental friendly feature make the ultrasonic welding process ideal for volume production of lithium-ion battery tab joints in electric vehicle manufacturing [24-27].

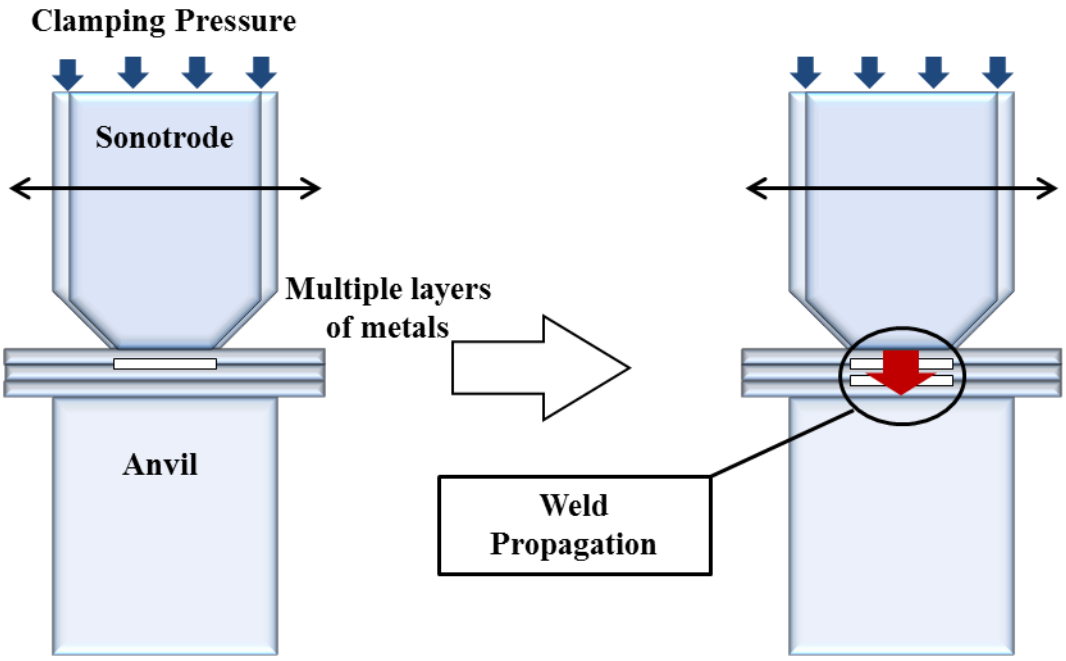

Figure 2.2 Weld propagation during ultrasonic welding process

2.3 Thermal and Electrical Effects on the Weld Joint

Application of the ultrasonically welded tab joints in lithium-ion battery packs requires performance stability under the fluctuation of the environmental temperature. Thermal stress is induced in a body when some or all of its components are not free to expand or contract in response to a uniform or non-uniform temperature change [28]. Thermal stress arises in Al-Cu weld joints due to dissimilar material properties in expansion coefficients. When the joint is subject to a temperature change, these two metals would expand by different amounts in accordance with the thermal elastic properties of the materials. The expansions will cause shear stress at the interface, which

may cause micro-cracks to form and propagate and eventually lead to failure of the joint [29-31]. Although they could withstand the peak stress in a single cycle, the metals will fail subject to a large number of successive thermal stress cycles. Therefore, the capability of the joint to endure thermal fatigue is an essential consideration of its vehicle application.

The electrical resistance of battery tab joints can be affected by the initial quality of the joints, as well as the deterioration due to fatigue or corrosion. Due to the high current demand during the vehicle operation, both the mechanical and electrical performance of the joint may be affected by repeated electrical cycles. Additionally, if micro-cracks were formed in the weld joint, a dramatic increase in the electrical resistance could lead to a high temperature by joule heating, which will result in equivalent thermal stress cycling. Consequently, an electrical cycling test could be needed to evaluate the fatigue performance of the battery tab joints.

2.4 PHYSICS-BASED LIFETIME PREDICTION MODEL

As mentioned above, the electrical resistance is influenced by microstructural changes of the investigated material and thus yields a corresponding change in resistance. Therefore, it is possible to use this physical quantity to evaluate the fatigue state as well as to predict the fatigue life of a specimen. Starke, Walther and Eifler introduced a new method for fatigue life prediction based on strain, temperature and electrical resistance measurements [32, 33]. In this method, the changes in temperature and electrical resistance were measured simultaneously with the plastic strain to evaluate the fatigue

mechanism on the basis of the generalized Morrow and Coffin-Manson curves. The exponential relation between the stress amplitude σ_a and the plastic strain amplitude ε_p was developed by Morrow as follows:

$$\sigma_a = K(\varepsilon_p)^n \qquad (2.1)$$

where K is the cyclic hardening coefficient and n is the cyclic hardening exponent. Then, the deformation-induced changes in electrical resistance ΔR can be equally used as the plastic strain amplitude to characterize the cyclic deformation behavior as follows:

$$\sigma_a = K_R\,(\Delta R)^{n_R} \qquad (2.2)$$

where K_R and n_R are the cyclic hardening coefficient and the cyclic hardening exponent corresponding to the electrical resistance change.

The generalized form of the relation between the stress amplitude and the fatigue life known as the S – N curve was introduced by Coffin-Manson as follows:

$$\sigma_a = \sigma_f\,(N)^b \qquad (2.3)$$

where σ_f is the fatigue strength coefficient and b is the fatigue strength exponent. Consequently, from Equation (2.2) and (2.3), the fatigue life of the specimen can be obtained as

$$N = \left[\frac{K_R}{\sigma_f}\,(\Delta R)^{n_R}\right]^{\frac{1}{b}} = A_R\,(\Delta R)^{b_R} \qquad (2.4)$$

where A_R and b_R are the two constants that can be determined from the experimental data. Therefore, if the change in electrical resistance corresponding to the number of cycles is known, the fatigue state of the specimen can be evaluated and the fatigue life can also be predicted accordingly.

This method replaces the plastic strain amplitude by the deformation-induced electrical resistance change in order for the characterization of the fatigue properties of the specimen under cyclic tensile load. In particular, for materials with a small plastic deformation, the measurement of electrical resistance yields an equivalent fatigue assessment as well as a fatigue life prediction based on the Morrow and Coffin-Manson equations. However, the power law relation between the plastic strain and the number of cycles characterized by Coffin-Manson is valid for low-cycle fatigue with the stress amplitude high enough for plastic deformation to occur. Additionally, the electrical resistance relies on the length, cross-sectional area and the electrical resistivity of the material. Therefore, a new relationship between the electrical resistance and the plastic strain amplitude needs to be developed in order to use the electrical resistance change to substitute the plastic strain measurement. At the weld joint, in addition to the plastic deformation, fatigue damage propagation also needs to be considered. Consequently, the electrical resistance change should be a function of plastic deformation as well as the fatigue growth rate on the weld joint.

Chapter 3: An Electrical Resistance Based Fatigue Model

3.1 INTRODUCTION

Many theories and models have been developed for fatigue life prediction for homogeneous materials [12]. The fatigue life of a metallic material is generally described by an S–N curve, also known as the Wöhler curve. When a cyclic stress is applied to a material sample and results in crack initiation, the crack growth rate can be related to the number of stress cycles using a power law function [8, 9]. Comparing to the crack growth fatigue model, the continuum damage mechanics (CDM) approach is relatively new, and has been used to postulate that the fatigue damage per cycle can be evaluated with a function of load condition and damage state. With the CDM formulation, the fatigue life of material can be predicted by measuring a physical parameter, such as temperature, electrical potential, electrical resistance, micro-hardness, toughness, and elastic modulus that can be used to represent the damage accumulation [10, 11, 13, 14]. Among all the physical parameters, electrical resistance has received substantial attention due to simple measurement setup and nondestructive nature. Recently, electrical resistance has been increasingly used in place of mechanical strain for fatigue life evaluation for high complexity materials, e.g., metal composites, as well as under more extensive cyclic loading conditions [15, 16]. Since it is strongly affected by the damage state, the electrical resistance of a material sample should show a characteristic trend representing the damage evolution, which can then be used to predict the fatigue life of the sample [17, 18, 32, 33].

In this chapter, an electrical resistance-based fatigue analysis is performed on lithium-ion battery tab joints made with ultrasonic welding. Similar to metallic materials, the electrical resistance of these ultrasonic welds strongly depends on the weld configuration, quality, and crack growth. A fatigue life model is developed using the continuum damage mechanics formulation. The damage variable is defined and related to the increase of electrical resistance of the ultrasonic welds, which can be used to predict the remaining fatigue life with the electrical resistance measurements.

3.2 Electrical Resistance Based Fatigue Life Prediction

Figure 3.1 shows a schematic of an ultrasonically welded battery joint sample under study. Three rectangular welds were made at the same time using one set of ultrasound horn and anvil. Since these welds are nominally identical, a single weld is analyzed without loss of generality. The loading condition of the sample is tensile-shear, with the tensile force shown as F_a. According to fracture mechanics, an isotropic damage variable, D, can be defined as [34, 35]:

$$D = \frac{A_d}{A} = 1 - \frac{A_e}{A} \qquad (3.1)$$

where A is the apparent area with side dimensions of X and Y, A_d is the damaged area of the joint, A_e is the effective load-bearing area (the same as electrical current bearing area), and $A_e = A - A_d$. In this study, A is assumed to be the initial bonded area of the ultrasonic joint, and therefore, a constant. A_e is changing due to damages such as crack initiation and growth. As shown in Fig. 3.1(b), the electrical resistance of the joint can be written as:

$$R = \frac{\rho t}{A} \qquad (3.2)$$

where *t* is the thickness of the weld and ρ is the electrical resistivity of the joint material.

Since the damage at the interface may not be distributed uniformly in the joint, the electrical resistance of the damaged area is regarded as inhomogeneous [18]. Therefore, the resistance after a certain amount of damage evolution can be written as:

$$R' = \int_{t'} \left(\int_{A'_e} \frac{1}{\rho'} dA'_e \right)^{-1} dt' \qquad (3.3)$$

where A'_e, $t'$and ρ' are the current conducting area, thickness of the weld, and electrical resistivity of the damaged interface, respectively.

During the fatigue process of a sample, plastic deformation could occur, which could also affect the electrical resistance. This plastic deformation effect needs to be excluded from the resistance change due to fatigue damage. As shown in Fig. 3.1(c), the shear stresses on the joint can be converted to equivalent principal stresses,

$$\sigma_a = \tau_a = \frac{F_a}{A} \qquad (3.4)$$

Assuming that the initial weld area changed from A to A' due to plastic deformation, the deformed area can be written as:

$$A' = x'y' = (1 - (1+\nu)\varepsilon_p) x\, y = (1 - (1+\nu)\varepsilon_p) A \qquad (3.5)$$

where ν is Poisson's ratio, and

$$\varepsilon_p = \frac{\sigma_a}{E'} \qquad (3.6)$$

E' is an equivalent modulus for plastic strain due to fatigue. The thickness *t* becomes

$$t' = (1 + (1+\nu)\varepsilon_p) t \qquad (3.7)$$

Since the area that conducts electrical current is assumed to be equal to the area that bears the mechanical load, the change of the effective area dA'_e can be expressed as:

$$dA'_e = (1 - D)dA' = (1 - D)\left(1 - (1 + \nu)\varepsilon_p\right)dA \quad (3.8)$$

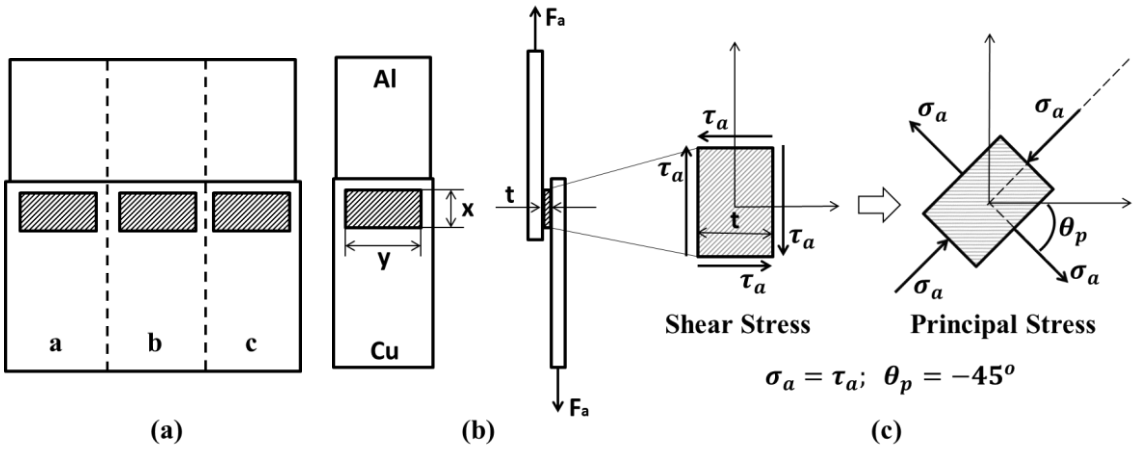

Figure 3.1 (a) A schematic a battery tab joint in this study, (b) a single weld joint, and (c) the loading condition of the joint

Substituting Eqs. (3.7) and (3.8) into Eq. (3.3), R' can be expressed as:

$$R' = (1 + (1 + \nu)\varepsilon_p)t)\left[\int_{dA}\frac{1}{\rho'}(1 - D)\left(1 - (1 + \nu)\varepsilon_p\right)dA\right]^{-1} \quad (3.9)$$

By assuming a uniform damage distribution and constant plastic strain at each time step, electrical resistance of the damaged joint, R', can be simplified into:

$$R' = \frac{\rho'\left(1+(1+\nu)\varepsilon_p\right)t}{(1-D)\left(1-(1+\nu)\varepsilon_p\right)A} = \left[\frac{1+(1+\nu)\varepsilon_p}{(1-D)\left(1-(1+\nu)\varepsilon_p\right)}\right]\left(\frac{\rho'}{\rho}\right)R \quad (3.10)$$

where R is the initial resistance of the joint. The damage variable can then be obtained as:

$$D = 1 - \left(\frac{1+(1+\nu)\varepsilon_p}{1-(1+\nu)\varepsilon_p}\right)\left(\frac{\rho'}{\rho}\right)\left(\frac{R}{R'}\right) \qquad (3.11)$$

Assuming the plastic deformation is small and there is no change in the electrical resistivity due to fatigue damage, the damage variable D can be simplified as:

$$D \approx 1 - \frac{R}{R'} = \frac{\Delta R}{R'} \qquad (3.12)$$

where ΔR is the change of electrical resistance from the initial state to the damaged state.

According to Marco and Starkey, Manson, and Chaboche [36-38], the damage evaluation rate can be represented using a general functional form as:

$$dD = D^{\alpha}\left[\frac{\sigma_a}{M(\tilde{\sigma})}\right]^{\beta} dn \qquad (3.13)$$

where σ_a and n are the stress amplitude and the number of fatigue cycles, respectively. The parameters α and β are constants that depend on thestress state and material properties. The function $M(\tilde{\sigma})$ has a linear dependency on the mean stress $\tilde{\sigma}$ and can be expressed as [36]

$$M(\tilde{\sigma}) = M_1\tilde{\sigma} + \sigma_0 \qquad (3.14)$$

where M_1 is a constant and σ_0 is the lowest stress during the cyclic loading. By separation of variables, this equation can be represented as:

$$D = \left[(1-\alpha)\left(\frac{\sigma_a}{M(\tilde{\sigma})}\right)^{\beta} n\right]^{\frac{1}{1-\alpha}} \qquad (3.15)$$

Comparing Eq. (3.12) to Eq. (3.15), a relative resistance increase ratio can be found as

$$\frac{\Delta R}{R} = \frac{D}{1-D} = \frac{\left[(1-\alpha)\left(\frac{\sigma_a}{M(\tilde{\sigma})}\right)^{\beta} n\right]^{\frac{1}{1-\alpha}}}{1-\left[(1-\alpha)\left(\frac{\sigma_a}{M(\tilde{\sigma})}\right)^{\beta} n\right]^{\frac{1}{1-\alpha}}} \qquad (3.16)$$

Note in Eq. (3.16) the joint fails when the damage variable D approaches to one. This is equivalent to that ΔR approaches infinity, which implies that the joint has broken. Equation (3.16) has three parameters α, β, and M_1 that need to be determined with experimental data from fatigue life tests.

In vehicle dynamics, the battery tab joint may experience a variety of stress amplitudes. If the crack growth rate is assumed to be independent of the pre-damaged area, which means that the joint has no memory effect, the electrical resistance change after the time period t should be cumulative. Infinitesimally small change in electrical resistance dR at the time period dt depends on the stress amplitude $\sigma_a(t)$ and the mean stress $\tilde{\sigma}(t)$. Therefore,

$$\frac{dR}{R_0} = \frac{\left[(1-\alpha)\left(\frac{\sigma_a(t)}{M(\tilde{\sigma}(t))}\right)^{\beta} dt\right]^{\frac{1}{1-\alpha}}}{1-\left[(1-\alpha)\left(\frac{\sigma_a(t)}{M(\tilde{\sigma}(t))}\right)^{\beta} dt\right]^{\frac{1}{1-\alpha}}} \qquad (3.17)$$

By integration of both sides of the equation, the resultant electrical resistance R_f becomes a function of the initial resistance R_0, σ_a and $\tilde{\sigma}$ as follows.

$$R_f = R_0[1 + H(t)] \qquad (3.18)$$

where $H(t) = \int_0^t \frac{\left[(1-\alpha)\left(\frac{\sigma_a(\tau)}{M(\tilde{\sigma}(\tau))}\right)^{\beta} d\tau\right]^{\frac{1}{1-\alpha}}}{1-\left[(1-\alpha)\left(\frac{\sigma_a(\tau)}{M(\tilde{\sigma}(\tau))}\right)^{\beta} d\tau\right]^{\frac{1}{1-\alpha}}}$

3.3 SUMMARY

Equation (3.18) represents a continuous method to model the initial crack as well as the propagation of fatigue damage under the specified stress amplitude and the mean

stress profile. Theoretically, when time increases, the resistance approaches infinity corresponding to the break of the joint. Further analysis and a comparative study with the experimental data will be discussed in Chapter 5.

Chapter 4: Experimental Setup and Procedure

Mechanical fatigue life tests were conducted with Al-Cu battery tab joints made with three different ultrasonic welding conditions, as shown in Table 4.1. These samples were designated as under-weld, nominal-weld, and over-weld, respectively, depending on their welding energy and time. The clamping force was fixed at 1200 N and the vibration amplitude was set at two, which is a coded level corresponding to amplitude in micrometers. Monotonic tensile shear tests were also performed on these samples, with the peak loads provided in the table. On average, the nominal-weld joints showed the highest tensile strength, while over-weld joint showed the lowest.

Table 4.1 Welding conditions of the joints

Weld Type	Energy (J)	Time (sec)	Clamping force (N)	Amplitude Level	Peak Tensile Load (N)
Under-Weld	150	0.12	1200	2	855
Nominal-Weld	400	0.22	1200	2	1025
Over-Weld	800	0.37	1200	2	763

Each sample was cut into three individual sections with a low speed diamond wheel saw and labeled as shown in Fig. 3.1(a). The samples were loaded on a dynamic mechanical analyzer (Bosh ElectroForce 3300) and tested at room temperature. The four-probe resistance measurement method was used with a micro-Ohm meter (Agilent 34420a) to measure the electrical resistances of the welds. The wires were attached 50 mm apart across the weld area. Each sample was insulated from the clamps in order to

minimize any possible electrical interference from the machine. Initial resistance of each sample was measured before testing and this value was corrected in the resistance data. A preprogrammed, cyclic tensile load at a certain frequency was applied to the sample while the electrical resistance of the weld was measured. The measurements were recorded at fixed time intervals with a data acquisition system (DAQ) through a GPIB-USB interface as shown in Fig. 4.1. Baseline tests were conducted to verify that the resistance change was in fact due to the fatigue of the ultrasonic welds instead of the base metal and the wires attached to the sample.

The test provides a curve of electrical resistance change (ΔR) versus the number of loading cycles (N), which indicates the fatigue effect on the electrical resistance due to the microstructural change in the weld. There are three welding locations on a single tab joint marked as **a**, **b** and **c** in Fig. 3.1 (a) and the weld quality at these three spots may vary due to possible difference in clamping pressure resulted from parallelism error of the ultrasound horn and anvil. All three types of joints at different welding locations were tested under three constant stress amplitudes of 3 MPa, 4 MPa and 5 MPa in order to present a wide range of data to the developed model. These fatigue testing conditions are shown in Table 4.2. The CATs were performed with a sinusoidal tensile load at a frequency of 50 Hz.

Both constant amplitude and linearly varying loads were used for the fatigue tests. The loads for constant amplitude tests (CATs) translated to shear stresses of 2-6 MPa. The frequency of the CATs was set at 50 Hz. Two other types of tests with linearly-varying loads were also used in the study. The load increment test (LIT) was conducted

with a stepwise stress increment of 0.25 MPa, starting from 0.75 MPa until failure. Within each step, the frequency of the cyclic load was set at 25 Hz and the step size was 5000 cycles. The variable load test (VLT) was performed with both stress increments and decrements within $3\ \text{MPa} \leq \sigma_a \leq 4\ \text{MPa}$ in a periodic manner. Again, each stress increment or decrement was 0.25 MPa, the frequency of the fatigue test was 25 Hz, and the step size was 5000 cycles. The fatigue test conditions using the three different types of loads are summarized in Table 4.3. All the tests were performed in a tensile-tensile mode with a preload of 0.25 MPa.

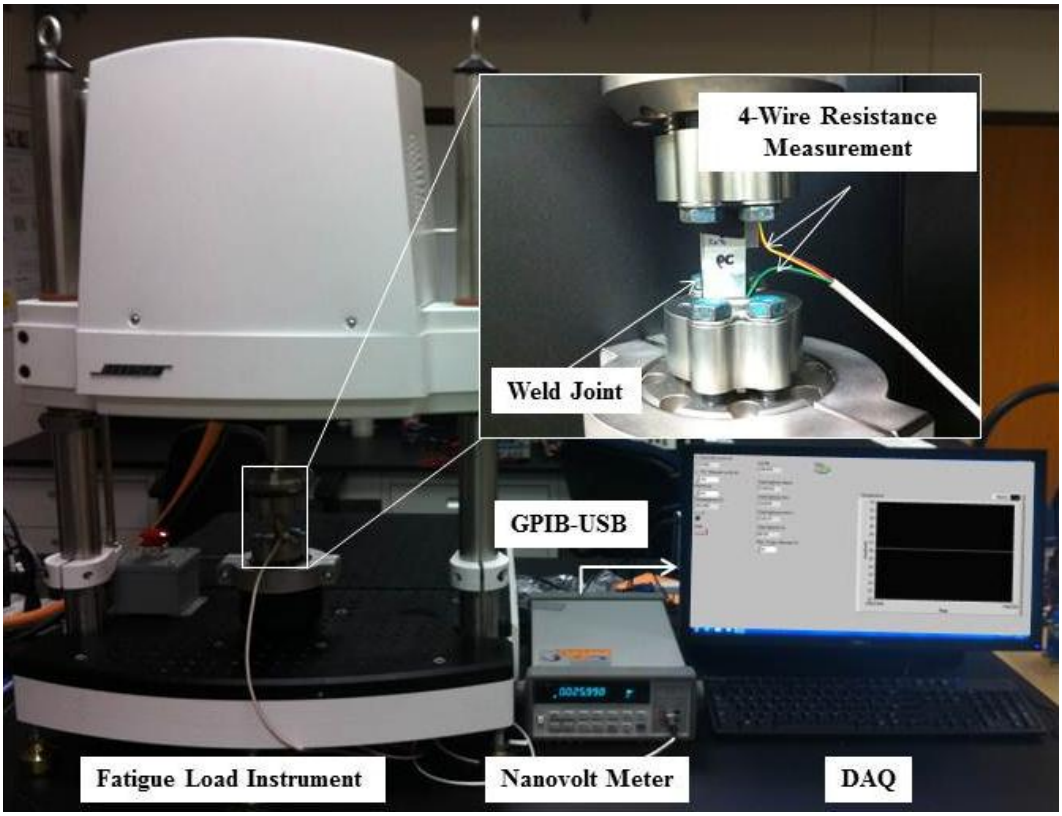

Figure 4.1 Experimental setup for the electrical resistance based fatigue test

Table 4.2 CAT fatigue testing conditions

No.	Weld Location	Welding Condition	Stress Level (MPa)
1	a	Under-Weld	3
2	a	Nominal-Weld	5
3	a	Over-Weld	4
4	b	Under-Weld	5
5	b	Nominal-Weld	4
6	b	Over-Weld	3
7	c	Under-Weld	4
8	c	Nominal-Weld	3
9	c	Over-Weld	5

Table 4.3 Load conditions of the fatigue tests

Load type	Amplitude range (MPa)	Frequency (Hz)	Δ Load (MPa)	Step size (Cycles)
Constant amplitude (CAT)	2-6	50	0	N/A
Load increment (LIT)	>0.75	25	0.25	5000
Variable load (VLT)	3-4	25	0.25	5000

Chapter 5: Results and Discussion

5.1 Fatigue Life Assessment

The results from constant amplitude tests (CATs) were used to construct ΔR-N and S-N curves for joints made under different welding conditions. Figure 5.1 shows the results for under-welds. As shown in Fig. 5.1 (a), the electrical resistance of the joints all gradually increased until failure. Once the failure occurred, the resistance increased rapidly to infinity. At 2 MPa, the under-weld joint achieved a fatigue life of more than 10^6 cycles. The fatigue life decreased as the stress increased. The S–N curve in Figure 5.1 (b) shows a familiar trend of fatigue life as related to applied stress. Figure 5.2 shows the results for nominal-welds, which exhibited a relatively higher endurance limit compared to the under-welds. The fatigue life was again more than 10^6 cycles at the stress level of 3 MPa, as shown in Fig. 5.2 (a). The S–N curve in Fig. 5.2 (b) shows the same trend as seen in Fig. 5.1 (b). For over-welds, most samples exhibited a stable increase in electrical resistance before failure. The fatigue life was more than 10^6 cycles at the stress amplitude of 3.5 MPa, as shown in Fig. 5.3 (a). The S–N curve in Fig. 5.3 (b) reveals an almost linear trend between the stress amplitude and fatigue cycle. This was due to the fact that the over-weld samples had a much longer fatigue life than under-welds and nominal-welds with the stress amplitudes tested. Comparing these ΔR-N and S-N curves, it is confirmed that the electrical resistance increases characteristically with loading and welding conditions and that this increase can be used for fatigue analysis of the battery tab joints.

Three different effects including welding energy, welding location and stress amplitude were considered in this study. Figure 5.4 present the experimental results based on fatigue life. Location **a** shows the highest vulnerability while **b** and **c** exhibited almost equal fatigue life. Therefore, according to the 3-level factorial design, over-welded joints have the longest fatigue life compared to the other two types, which is the same as the above-mentioned results. Also, higher stress causes lower fatigue life as expected. Interestingly, location of weld shows significant effect. Since they were made using the same set of tool under the same welding condition, the three welds should have the same property. However, there could be slight misalignment between the ultrasound horn and anvil, resulting in the quality difference.

The comparison of the three types of joints showed predominant advantage of the over-weld joint for its longer fatigue life as well as the most stable increase in electrical resistance under the same stress level. More importantly, it confirms that all three types of joints show increase in electrical resistance corresponding to increasing number of loading cycles, which means that the electrical resistance can used as a damage variable to predict the fatigue state using the developed prediction model.

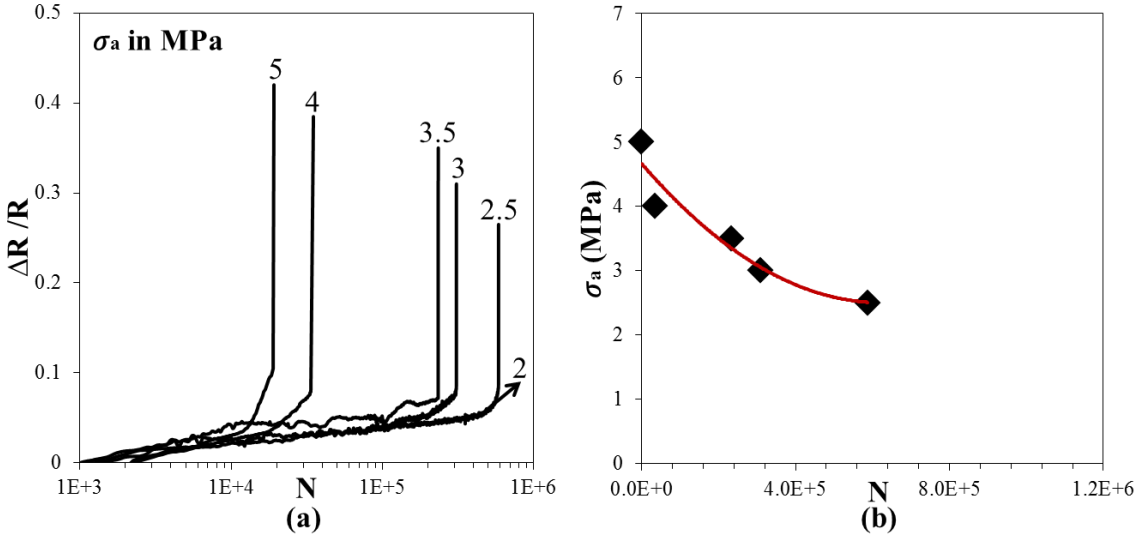

Figure 5.1 ΔR–N curve (a) and S–N curve (b) for CATs on under-weld joints. The stress levels σ_a's are shown in (a).

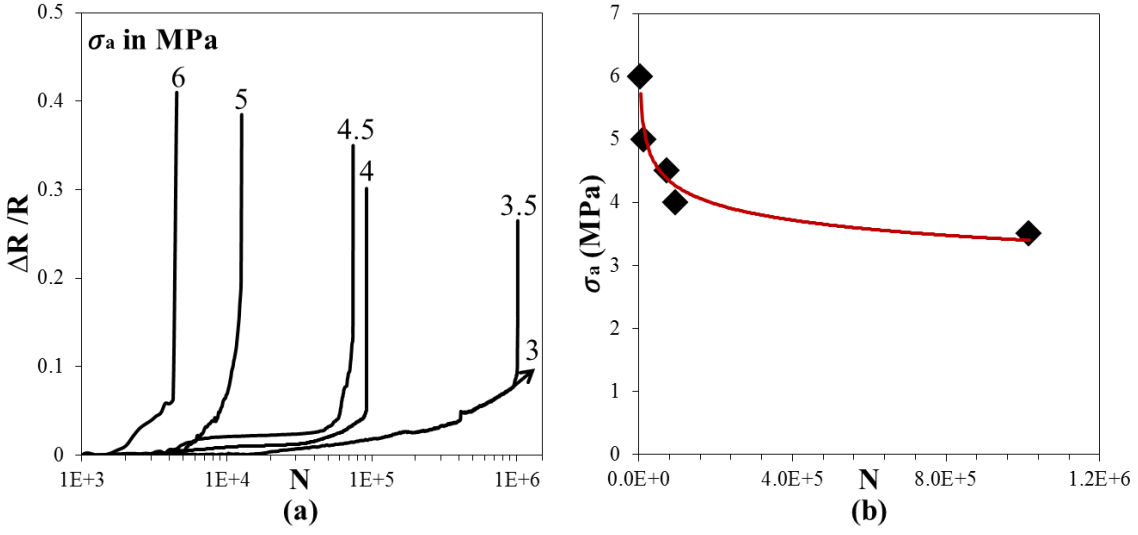

Figure 5.2 (a) ΔR–N curves and (b) S–N curves from CATs of nominal-welds. The stress levels σ_a's are shown in (a).

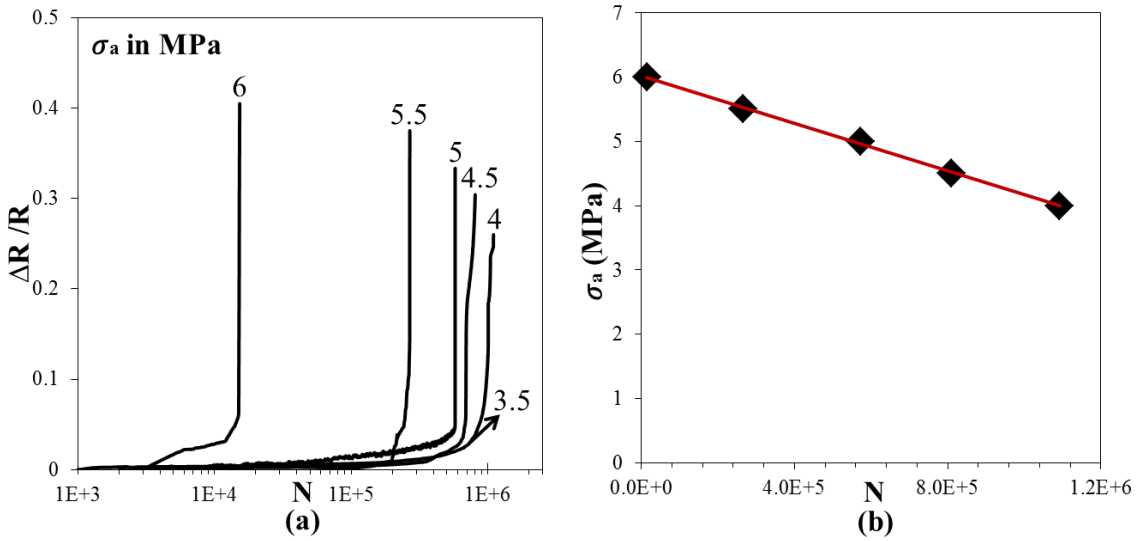

Figure 5.3 (a) ΔR–N curves and (b) S–N curves from CATs of over-welds. The stress levels σ_a's are shown in (a).

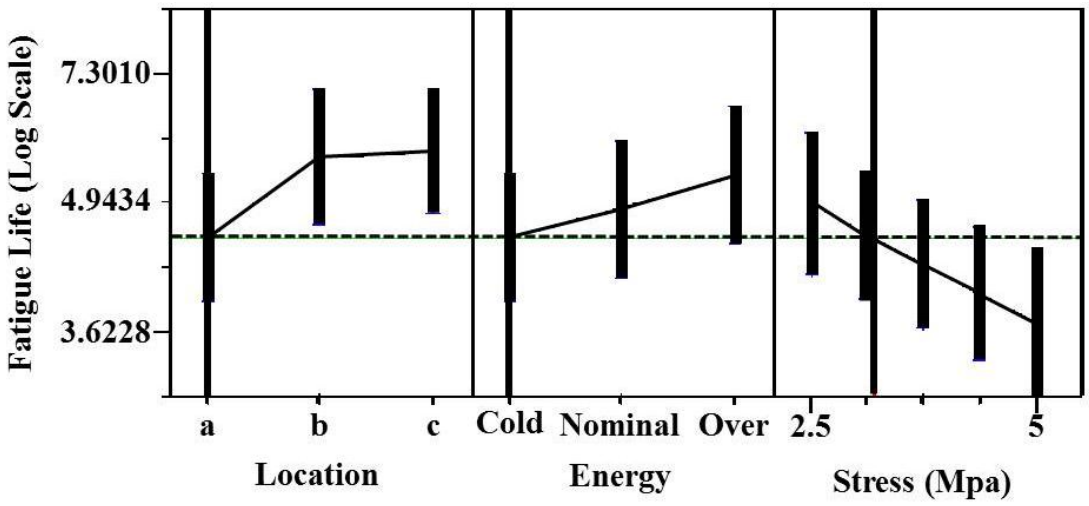

Figure 5.4 Result of 3-level factorial design

5.2 FAILURE MODES

Figure 5.5 shows important failure modes of the Al-Cu battery joints. Most of the joints failed at the weld zone under different stress amplitudes. When the stress amplitude is 5 MPa, all three types of Al-Cu joints tend to break apart completely on the weld zone as shown in Fig. 5.5 (a). When the stress level is at 4 MPa, failure occurs close to the edge of the weld zone as shown in Fig. 5.5 (b). However, when the stress amplitdue is 3 MPa, which is close to the endurance limit of the joint, all the weld joints would eventually fail at the aluminum sheet instead of on the welded area as shown in Fig. 5.5 (c).

Under-weld **Nominal-weld** **Over-weld**

(a)

Under-weld **Nominal-weld** **Over-weld**

(b)

Under-weld **Nominal-weld** **Over-weld**

(c)

Figure 5.5 Failure modes of three types of joints at the stress amplitude $\sigma_a = 5$ MPa (a), $\sigma_a = 4$ MPa (b), and $\sigma_a = 3$ MPa (c).

5.3 PARAMETER ESTIMATION AND MODEL FITTING

Equation (3.16) characterizes the relationship between the number of loading cycles and the change in electrical resistance if the stress level is a known constant. Conversely, if the resistance change of the specimen is measurable, the fatigue state can be assessed and the remaining life cycles can be predicted at any given point of time. This estimation and prediction can be performed iteratively as the number of cycle increases. The more data to include in the estimation, the more accurate the prediction will be. In this study, electrical resistance up to certain time was used to estimate the parameters of the fatigue life model. The model was then used for prediction. We compare the predicted resistance increases with the measured ones at different points of time during the fatigue test. The estimation was based on the Levenberg–Marquardt algorithm (LMA) for minimization [39, 40]. The objective function was defined as

$$S(\alpha, \beta, M_1) = \sum_{i=1}^{m} \left[\Delta R_i - \Delta R\left(\left[\sigma_{a_i}, \tilde{\sigma}_i, n_i\right]', [\alpha, \beta, M_1]'\right)\right]^2 \quad (5.1)$$

where m is the number of available data points, ΔR_i is the measured resistance increase and $\Delta R([\sigma_{a_i}, \tilde{\sigma}_i, n_i], [\alpha, \beta, M_1])$ is the predicted value, with $\sigma_{a_i}, \tilde{\sigma}_i,$ and n_i as the stress amplitude, mean stress, and number of cycles, respectively. Since M_1 is a constant coefficient determining the stress state and there is a strong dependency between β and M_1, M_1 is fixed as a constant in this study. By trial and error, M_1=20 was taken to yield good fitting results. Therefore, only two model parameters α and β need to be determined using the experimental data.

Figure 5.6 shows the fitted results of the damage variable D as a function of cycle fraction (N/N_f) for typical test samples under different welding and fatigue loading conditions. N_f is the fatigue life of the corresponding sample. It can be seen that the model fitted well with all the experimental data, indicating that it is capable of describing the damage evolution under various conditions. It is also seen that the shape of the damage curve is affected by both the stress level and weld quality. The D curve shows a higher curvature for a weaker weld and at a lower stress level. When the stress is high and the weld is over-weld, the D curve has a smaller curvature. More importantly, there appears to be a threshold D value, beyond which the weld would fail. This D value is a function of the applied load. For example, at 3 MPa the welds are close to fail when $D \approx 0.5$; at 4 MPa failures occur around $D \approx 0.3$; and at 5 MPa the threshold is $D \approx 0.2$. The type of weld does not seem to have an effect on the threshold values.

Theoretically $D=1$ corresponds to failure as discussed earlier. However, when damage propagates to a certain point, the final failure of the joint happens very fast. Consequently the electrical resistance increases dramatically to infinity in a short time. Such a sudden increase is hard to capture using fitted models. Therefore, a certain threshold on the damage curve can be applied to determine when the failure would occur. As shown in Figure 5.6, the thresholds were taken when the fitted trend line reaches $N=N_f$, where N_f was the last data point in each of the plots. N_f was the fatigue life of the sample from the test. It was not included in the model fitting.

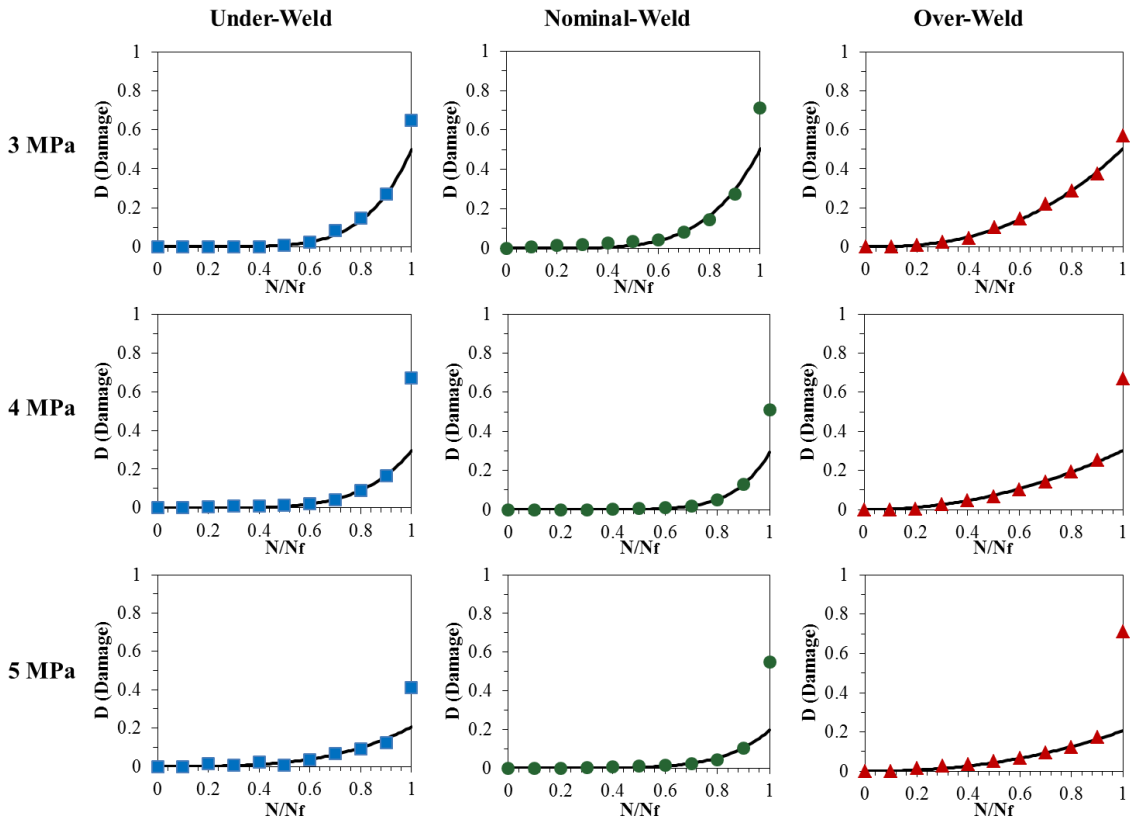

Figure 5.6 Comparison between prediction model and experimental data from CATs

After model fitting, the determined α and β values for various welding and loading conditions can be shown as in Fig. 5.7. In general different types of welds fell within different regions on the α-β plane. The α value varied from 0 to 0.4 for over-weld joints and from 0.5 to 0.9 for nominal-weld joints. The β value ranged between 5 and 8 for over-weld joints and from 3 to 6 for nominal welds. Under-weld joints exhibited a large variation, with α mainly within the range of $0.4 \leq \alpha \leq 0.9$ and β in the range of

$0 \leq \beta \leq 3$. By observation, α affects the rate of change of electrical resistance, while β is related to the fatigue life. In general, a smaller α means a slower increase of the resistance and a larger β implies a longer fatigue life. Therefore, it is interesting to see that the over-weld joints clustered at the lower-right corner of the plot, indicating that they were the strongest welds in terms of the fatigue life. Under-welds clustered at the upper-left corner, suggesting that they were the weakest. Nominal welds were in between the over- and under-weld joints. The performance of under-weld joints varied dramatically. Some behaved similarly to nominal-welds and others to over-welds. With α and β values, welds made under different conditions can be classified into groups, such as weak welds and good welds, based on their fatigue performance.

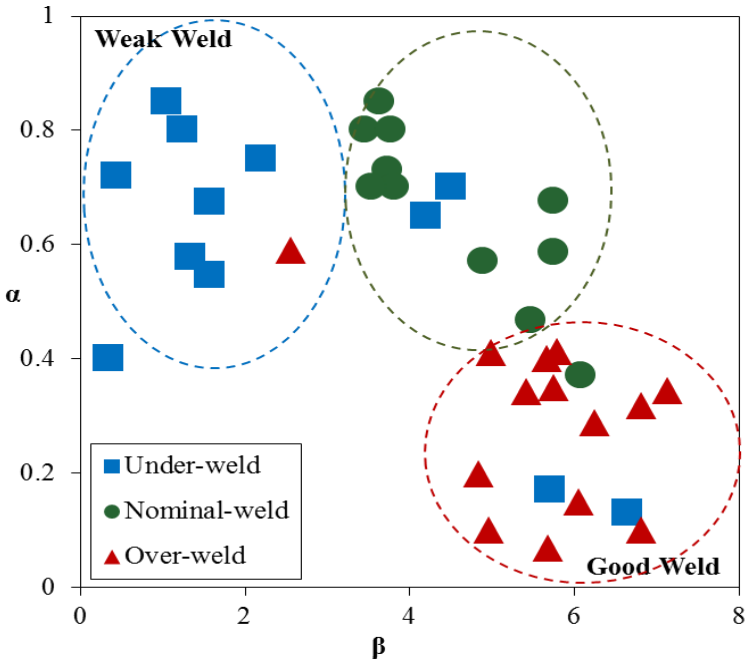

Figure 5.7 Estimated α and β values used to classify weld quality.

5.4 PREDICTABILITY OF THE FATIGUE MODEL

The estimation procedure defined in Eq. (5.1) can be performed iteratively as the number of fatigue cycle increases. At each time step the fitted fatigue model can be used for prediction. The predictability of the fatigue model was tested by using only a portion of the fatigue data for model fitting and the rest for validation. Figure 5.8 shows the results. The initial approximation of the model started with the fatigue data from 0 to $0.1N_f$ cycles. The model was updated as more data points became available. As can be imagined, the model prediction would become more accurate when more data points were used. In this case, the fitted model using data up to $0.6N_f$ could predict the final fatigue life well enough. This sample was a nominal weld loaded under constant stress amplitude of 4 MPa.

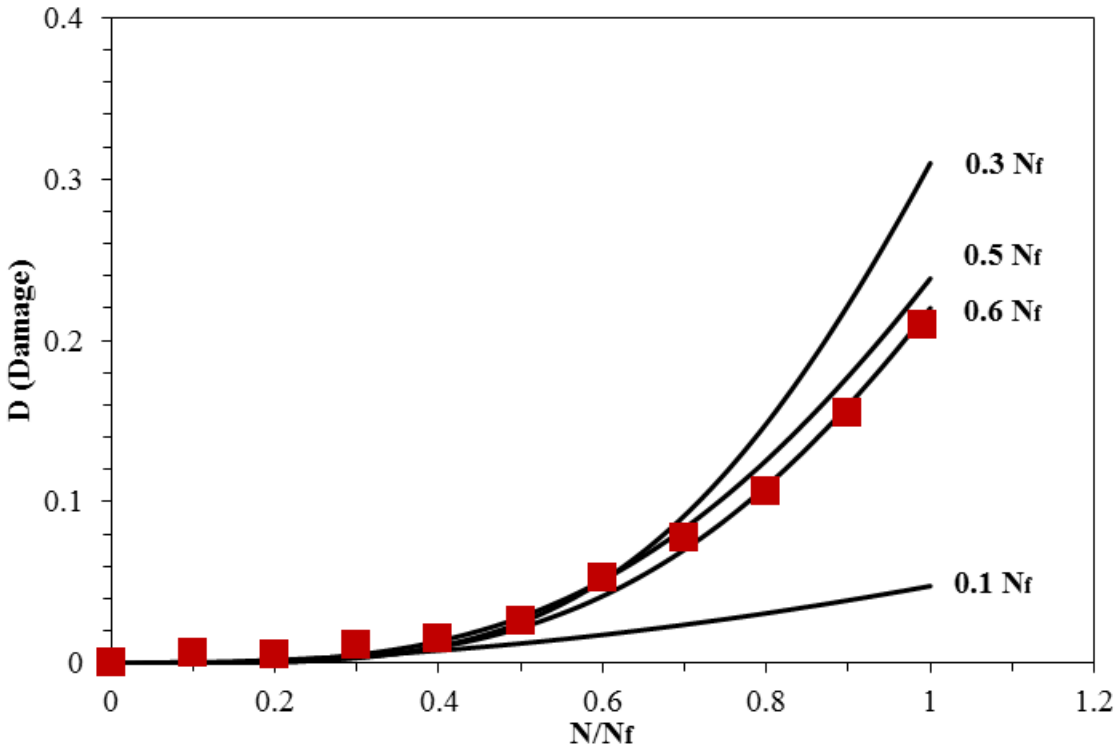

Figure 5.8 Comparison between model prediction and the experimental data for constant amplitude test at 4 MPa.

To further validate the model's ability for prediction, the loading stress was allowed to vary during the fatigue test. Equation (3.18) was used to compute the accumulative fatigue propagation of the weld samples. This was done under the assumption that the peak-to-peak stress amplitude $\sigma_a(t)$ and the mean stress $\tilde{\sigma}(t)$ at any time instance *t* are known. As shown in Figure 5.9, the model prediction for the load increment test approaches to the experimental measurements closely as more data points were used in the model estimation. With the first $0.5N_f$ cycles of data the model

prediction showed a good agreement with the experimental data for the remaining fatigue cycles.

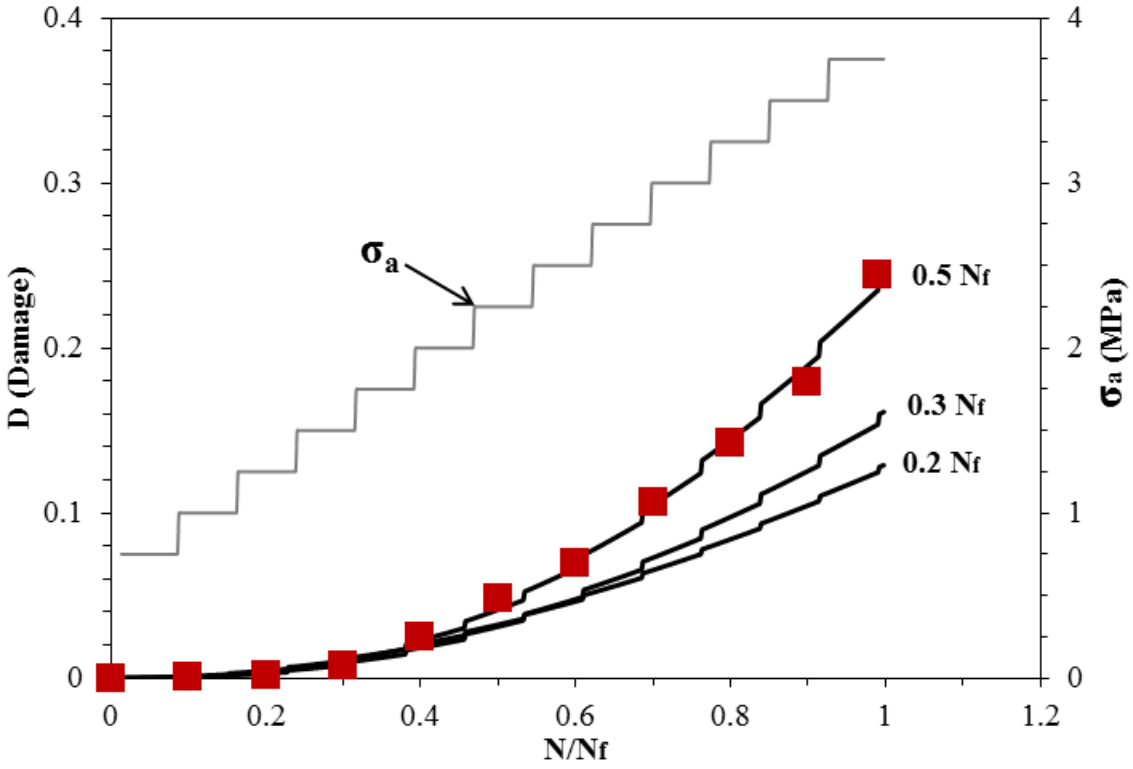

Figure 5.9 Comparison between model prediction and experimental results for a load increment test.

Figure 5.10 shows the prediction result for a sample in a variable load test, where the fatigue load varied between 3-4 MPa with a step-wise increment or decrement of 0.25 MPa. It can be seen that as the stress increased the damage variable increased rapidly, similar to that in the load increment test. As the stress decreased, the damage variable

continued to increase, however, at a much slower rate. The predicted damage increase using $0.5N_f$ of the data points captured the damage increase fairly well. There was a delay in following the trend at the event when the rate of damage increase started to change; however, the overall prediction still followed to the experimental measurements closely.

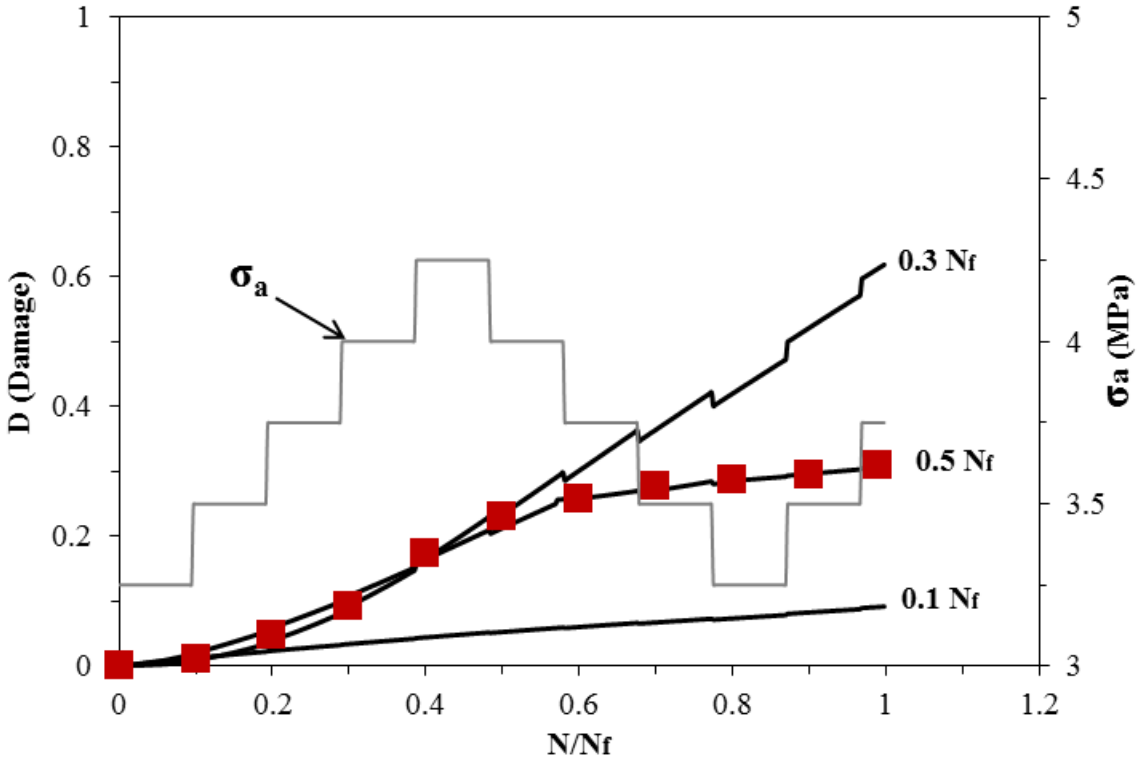

Figure 5.10 Comparison between model prediction and experimental results for a variable load test.

While the above results demonstrate that the developed resistance-based fatigue model can be used to predict the damage variable as the fatigue cycle increases, it should

be noted that a detailed study will be needed to determine a robust threshold for failure to occur. For the constant amplitude test, it seems that there exists a relation between the failure threshold and the stress level. The higher the stress level, the lower the failure threshold. From Eq. (3.1), an effective stress at failure can be defined as $\sigma_e = \frac{F_a}{A_e} = \frac{\sigma_a}{1-D}$. The constant amplitude test data in this study suggested that failures all occurred at $\sigma_e \approx 6$ MPa in this case. However, when the stress level varies, such as those in the load increment and variable load tests, the failure threshold need to be evaluated based on the accumulative effect of the varying stress. Furthermore, since the failure event happens in a relatively short time, the resistance, thus the damage variable, increases dramatically right before failure. Such a sudden increase presents a significant challenge for modeling and may require an adaptive model estimation and prediction scheme to solve. These tasks are beyond the scope of this study and will be addressed in the future.

5.5 SUMMARY

An electrical resistance-based fatigue analysis was performed on lithium-ion Al-Cu battery tab joints made with ultrasonic welding. From experimental result, it was observed that welding energy and welding time exhibited a strong effect on the fatigue performance of the battery tab joints. Over-weld joints performed better than nominal- and under-weld joints in fatigue and thus should be the first choice in battery pack manufacturing. In addition, the weld quality also varies by the welding location due to different clamping force applied during the welding process, which means a proper alignment of the tab joints is needed for better performance and longer fatigue life.

The electrical resistance change of ultrasonic welds relies on the initial weld quality, plastic deformation and crack growth on the weld zone, thus can be used to assess the fatigue behavior of the joints. Therefore, a fatigue life model was developed based on the electrical resistance change in order for the characterization of the fatigue state as well as for the prediction of the remaining life of the joints. The developed model showed agreement with the experimental data under various stress conditions, i.e., CAT, LIT, and VLT. Additionally, by classification of the two parameters of the fitted model, the weld quality of the joint can be identified accordingly and the results can be used as a guideline for the implementation of ultrasonic welding in mass production.

Chapter 6: Thermal and Electrical Fatigue Tests

6.1 Objectives

Battery tab joints in electric vehicles are subject to high fluctuation in temperature, which can drop as low as -40 °C in winter and rise up to 90 °C during operation. Differential expansion of the Al-Cu joints due to this temperature change may cause micro-cracks that will propagate through the joint area, which will eventually lead to failure of the joint due to a large number of successive thermal cycles. Therefore, the purpose of the thermal fatigue test is to evaluate the capability of the ultrasonically welded battery joints to endure thermal fatigue under the extreme environmental temperature cycling. In addition to the variation in temperature, the battery joints are also subject to high electrical current passing through the welded area due to the high current demand for the vehicle powertrain system. The purpose of the electrical cycling test is to simulate the current demand variation during vehicle operation to evaluate the fatigue performance of the battery tab joints under high electrical current cycling.

6.2 Finite Element Analysis (FEA) of the Thermal Stress

When there is a change in temperature, two elastic layers on the joint tend to expand unequally due to dissimilar material properties. An analytical solution is provided in Appendix – A, where internal thermal stress was replaced by externally applied axial forces with the interface under shear and tensile stresses [29]. Under the proper assumptions of initial and boundary conditions, a solution can be found numerically with

the maximum shear stress as 13.9 MPa at the free edge of the two bonded joints. The total equivalent tensile force was 27.7 N, which is much less than the endurance limit (100 N) of the Al-Cu joint. A finite element simulation model was developed using SolidWorks®. Aluminum and copper sheets were designed according to the real dimensions of the weld joint. Two metal sheets were bonded together with a fixed constraint on one end while allowing free expansion in vertical and horizontal directions on the other end. Fig. 6.1 shows the finite element mesh and deformed shape of the model under the temperature change from -40 ^{o}C to 90 ^{o}C with the maximum shear stress of 18.7 MPa occurred at the free edge.

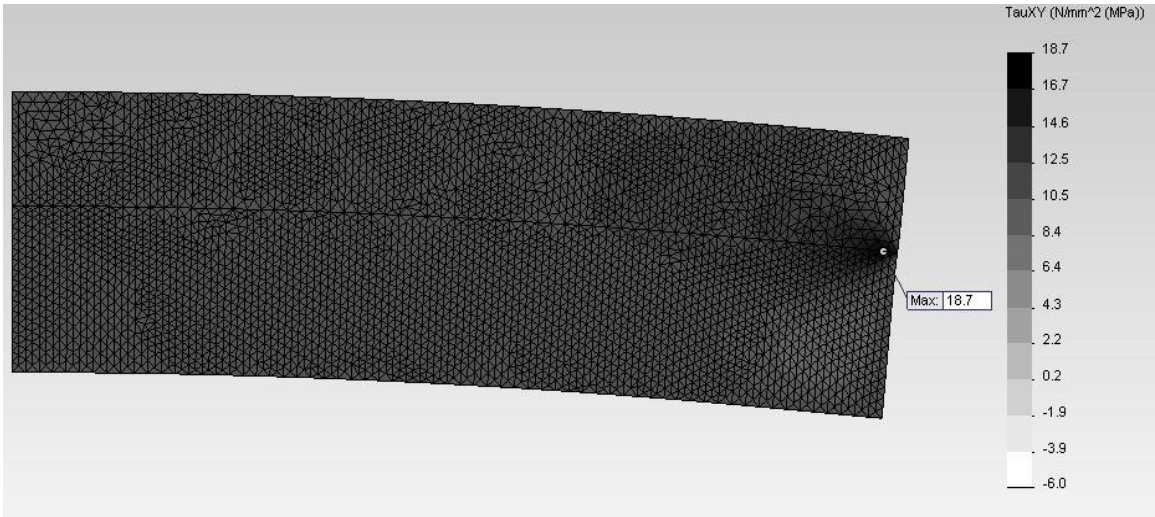

Figure 6.1 FEA simulation result

6.3 EXPERIMENTAL SETUP AND PROCEDURE

Thermal cycling test was conducted in an environmental chamber with a preprogramed temperature cycle between -40 °C and 90 °C as shown in Fig 6.2. Thermocouples were attached to the samples to monitor the actual change in temperature as shown in Fig. 6.3. Each cycle takes approximately 80 minutes. After each preset number of cycles, the electrical resistance of each tab joint was measured using the 4-wire measurement technique, which eliminates the effects of the resistance on the connecting wires as shown in Figure 6.4.

Electrical fatigue test was conducted simultaneously on multiple samples connected to the leads in series with a power supply tuned to cycle between 0 and 10 A at the frequency of 20 Hz, as shown in Fig. 6.5. A Labview controlled relay switch in Fig. 6.6 was used to pass current through the leads and to disconnect the circuit after a certain number of cycles. Then the electrical resistance was measured at successively increasing number of cycles using the 4-wire resistance measurement technique.

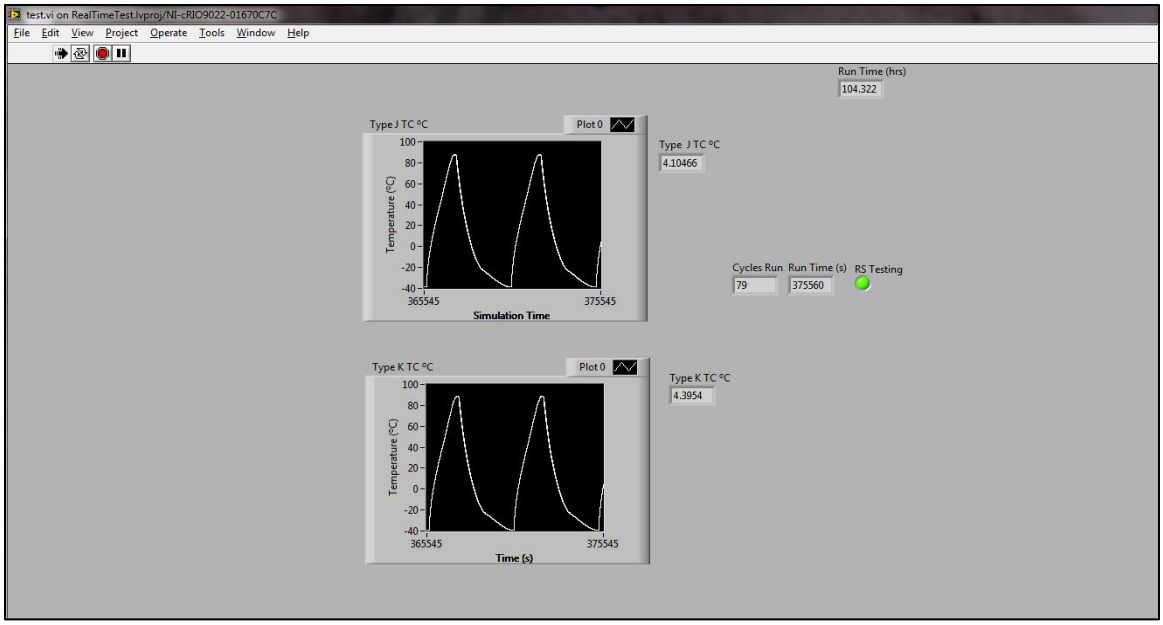

Figure 6.2 Labview front panel control for the environmental chamber

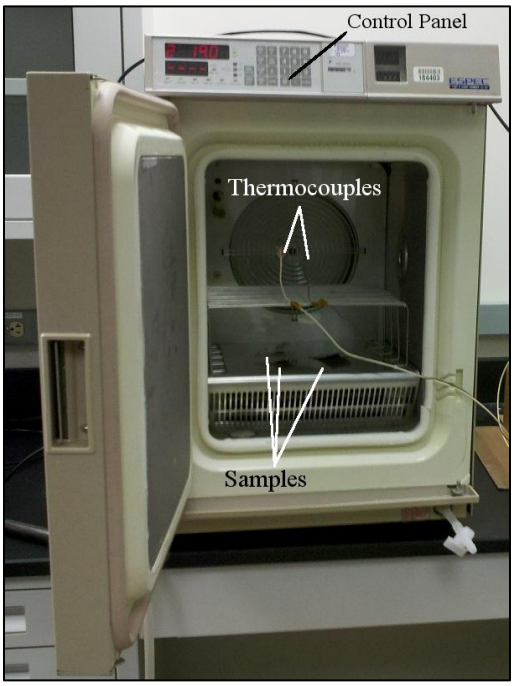

Figure 6.3 Thermal test setup in the environmental chamber

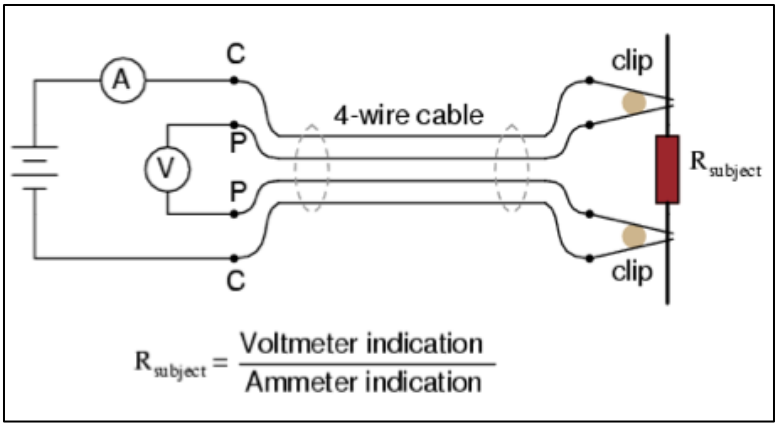

Figure 6.4 Diagram of 4-wire resistance measurement technique

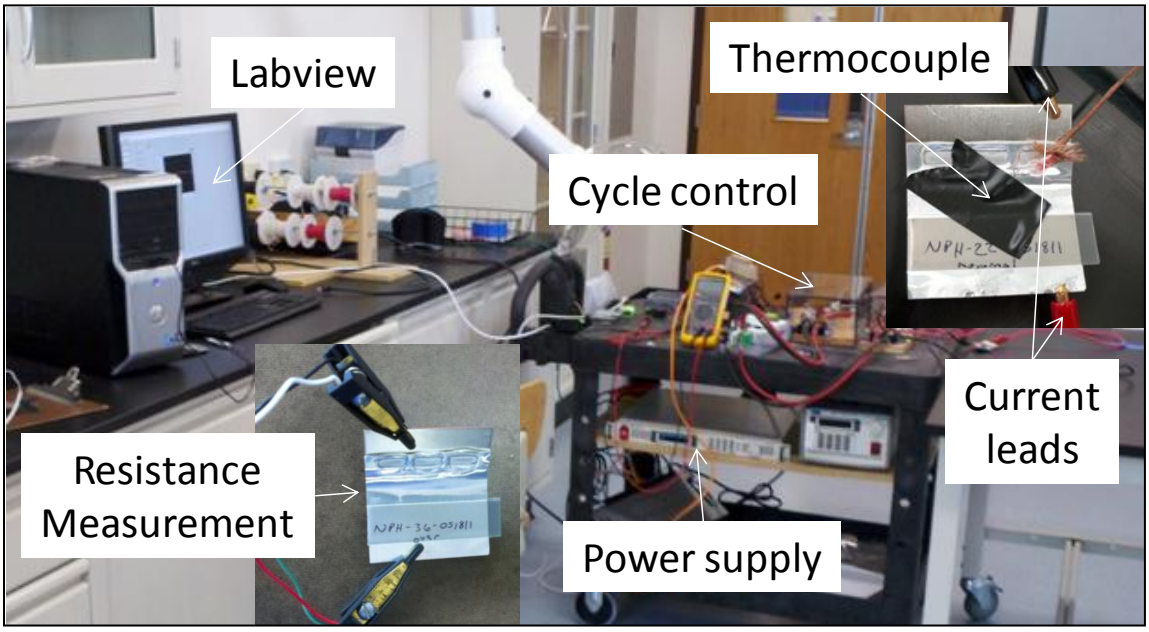

Figure 6.5 Electrical cycling test setup

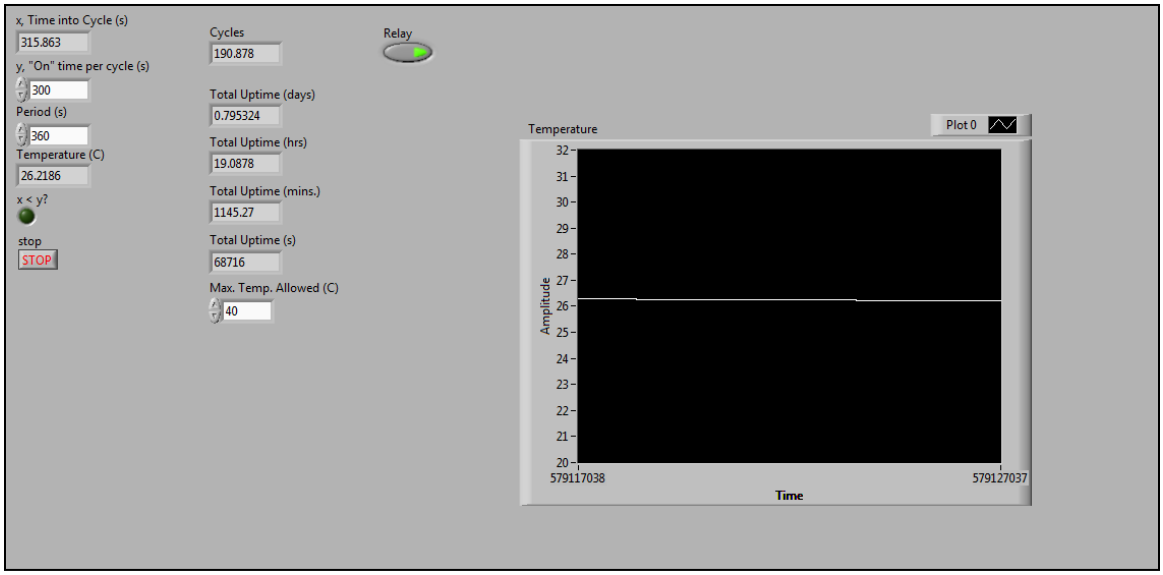

Figure 6.6 Electrical test control program

6.4 TEST RESULTS AND DISCUSSION

Table 6.1 presents the results of the electrical resistance change under the thermal cycling with the temperature range of from -40 ºC to 90 ºC. The test was conducted up to 396 cycles without showing any significant change in electrical resistance. For a further analysis of the thermal stress, an equivalent tensile force was calculated using both the analytical solution and the FEA within the temperature range from -40 ºC to 90 ºC. The maximum stress from analytical solution and FEA were 13.9 MPa and 18.7 MPa respectively. However, the average stress levels were much lower. The equivalent tensile force is thus less than 110 N, which is the endurance limit of the joint. Consequently, up to this point, thermal effect is not by itself a cause for significant changes in mechanical

and electrical properties of the weld joints.

For electrical cycling test, as shown in Table 6.2, there is a very small change in electrical resistance after at least 1,000,000 cycles. Therefore, electrical fatigue may not be a concern for the application of the Al-Cu joints in electric vehicles.

Table 6.1 Thermal cycling test results for -40-90 ºC

Under		Nominal		Over	
Cycles	R(μΩ)	Cycles	R(μΩ)	Cycles	R(μΩ)
0	11	0	12	0	13
18	11	18	12	18	11
126	12	126	9	126	10
200	12	200	10	200	12
300	11	300	11	300	11
396	13	396	9	396	10

Table 6.2 Electrical cycling test result

Cold-welded Joint			
Cycles	R_1 (μΩ)	R_2 (μΩ)	R_3 (μΩ)
0	13	11	12
10,000	12	11	11
100,000	11	10	12
1,000,000	11	10	11
Nominal-welded Joint			
Cycles	R_1 (μΩ)	R_2 (μΩ)	R_3 (μΩ)
0	11	11	11
10,000	10	11	10
100,000	12	10	12
1,000,000	12	11	12
Over-welded Joint			
Cycles	R_1 (μΩ)	R_2 (μΩ)	R_3 (μΩ)
0	11	10	12
10,000	13	11	11
100,000	11	11	11
10,00,000	12	13	13

6.5 SUMMARY

Thermal and electrical fatigue tests were conducted to simulate the fluctuation of the environmental temperature as well as the high variation of current demand during vehicle operation. The tests were performed on individual welds made using three different welding conditions: under-weld, nominal-weld and over-weld Al-Cu joints. In thermal fatigue tests, all three types of joints showed no significant increase in electrical resistance and thus may not be a concern for the battery tab joints. Electrical fatigue tests

also showed insignificant change in electrical resistance of the joint. Therefore, electrical fatigue may not affect the fatigue behavior of the battery joint for its application on electric vehicles.

Chapter 7: Summary and Conclusions

An electrical resistance based fatigue study was conducted in this research for ultrasonically welded lithium-ion battery tab joints by performing mechanical, thermal and electrical tests. An adaptive fatigue prediction model based on electrical resistance change was developed in order to characterize the fatigue behavior as well as to predict the remaining life of the battery joints. Conclusions are summarized as follows:

1) Welding energy exhibits a strong effect on the fatigue behavior of the battery tab joints. Over-weld joints perform better than nominal-weld and under-welded joints, even though they may have the lowest tensile strength. The resistance increase of over-weld joints also exhibits the highest stability compared to nominal and under welds.
2) Welding conditions also vary at different joint locations with one side showing high vulnerability under mechanical loading. Therefore, a proper alignment of the tab joints will improve the overall performance and extend the fatigue life of the entire battery system. Also, higher stress amplitudes leads to shorter fatigue life as expected.
3) The electrical resistance change of ultrasonic welds relies on the initial weld quality, plastic deformation and crack growth in the weld zone, thus can be used to assess the fatigue behavior of the joints. Therefore, a fatigue life model was developed based on the electrical resistance change for characterization of the fatigue state as well as for prediction of the remaining life of the joints. The developed model agreed well with the experimental data under various stress conditions, i.e., CAT, LIT, and VLT.

Additionally, by classification of the two parameters in the fitted model, the weld quality of the joint can be identified accordingly and thus can be used as the quality guideline for ultrasonic welding in mass production. This fatigue model can be further developed to monitor the fatigue state as well as to predict the remaining fatigue life of the battery tab joints for electric and hybrid electric vehicle applications.

4) Thermal tests were conducted in order to simulate the fluctuation of the environmental temperature for the application of the battery joints in electric vehicles. Experimental results showed insignificant change in electrical resistance of the joints. Therefore, thermal fatigue may not be a concern for the battery tab joints.
5) Electrical tests were conducted in order to simulate the current demand variation during vehicle operation to evaluate the fatigue performance of the battery tab joints under electrical cycling. Experimental results again showed insignificant change in electrical resistance of the joint. Therefore, electrical fatigue may not be a concern for the battery tab joints.

Chapter 8: Future Work

Battery pack manufacturing requires a large number of various joining processes and a monitoring system to evaluate the fatigue state as well as to predict the fatigue life, since the entire battery is a complex multidisciplinary system. This research focused on the smallest joining units of the batteries. The developed prediction model works well at the cell level. However, there is still work to improve the prediction model. Further study on the vehicle vibration and the environmental condition will allow for a more detailed model validation and application in electric vehicles. Additional static tensile tests can be conducted and compared with the fatigue test results in order to find the relation between the tensile strength and the fatigue life of the joint. Further study is needed on the welding process including clamping force, welding time and welding energy, which imposed a considerable effect on the fatigue property of the joint. Additional thermal and electrical fatigue tests may also be needed to confirm the findings in this study.

8.1 Application of the Prediction Model

The developed prediction model showed an excellent agreement with the experimental data under various tensile loading conditions. However, the model was derived under the assumptions of pure tensile loading condition and was validated correspondingly. However, in vehicles the battery joints will need to bear a variety of harsh loading conditions including tension, compression, bending, torsion, peeling, etc. Therefore, a more sophisticated mechanics model that involves the analysis of vehicle vibration, battery pack structure, and battery cell arrangements is needed in order to

develop a practical monitoring system for the entire battery pack.

8.2 TENSILE STRENGTH VERSUS FATIGUE LIFE

For metallic materials, a higher tensile strength normally corresponds to a higher endurance limit and a longer fatigue life. As shown in Table 4.1, the tensile strength of the over-weld joint is the lowest while nominal-weld joint showed the highest. But in the fatigue tests, over-weld joints performed best among the three types both in the longest fatigue life and smallest increase in electrical resistance. Due to high variation of weld quality in ultrasonic welding, this phenomenon needs further validation and more tensile tests will provide a better comparison among the three types of joints. If the experimental results are validated, a further study can be conducted to determine the correlation between the tensile strength and fatigue life of the joint.

8.3 EFFECT OF WELDING PARAMETERS

Three types of Al-Cu joints made under different welding conditions, i.e., welding energy and welding time, were studied in this research. Over-weld joints were found to have the largest fatigue life. This implies that a higher welding energy and a longer welding time lead to better performance of the joint. However, a detailed study on the welding parameters that could contribute to the best weld quality is lacking. In addition, three welds on a single tab were made using the same set of tooling under the same welding condition, thus should result in the same fatigue property. However, due to possible misalignment between the ultrasound horn and anvil, the weld quality varies at different locations discussed in Chapter 5. It means that these three parameters are all

imposing significant effects on the weld quality of the joint. Therefore, the weld parameters including energy and time should be studied together with alignment to achieve the best weld quality.

8.4 THERMAL AND ELECTRICAL FATIGUE TEST

Thermal and electrical fatigue tests were conducted in order to simulate the environmental and operating conditions of electric vehicles. The electrical resistance measurement was used to monitor the fatigue state of the battery joint with no significant change found so far. However, the thermal, electrical, and mechanical tests in this study were conducted separately. Possible interaction effects among these three load conditions cannot be observed. A fatigue test under the combined loads could provide a more realistic result for evaluation of battery tab joint life.

Appendix – A

Analytical Solution for the Thermal Stress

When there is a change in temperature, two elastic layers on the joint tend to expand unequally due to dissimilar material properties. The two layers can be assumed as two beams under axial and bending deformations with no slip at the interface. In this study, the internal thermal stress was replaced by externally applied axial forces with the interface under shear and tensile stresses, which is essentially the same approach taken by Goland and Reissner [29]. The two layers welded together were assumed to be of uniform thicknesses (t_1 and t_2), and with Young's moduli (E_1 and E_2), shear moduli (G_1 and G_2), Poisson's ratios (γ_1, γ_2), and the constant thermal expansion coefficients (α_1 and α_2) as shown in Fig. A.1. The forces acting on the elastic layers were assumed to be uniform and therefore, resulting in the corresponding shear and tensile stresses at the interface. Figure A.2 shows the moments and forces applied on an elemental segment dx.

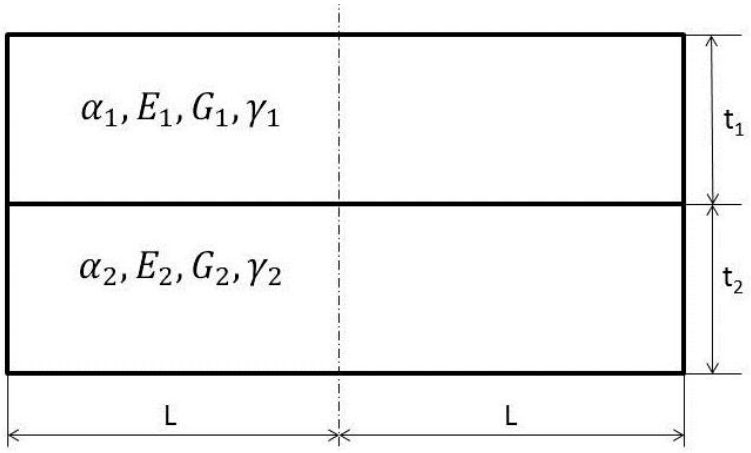

Figure A.1 Schematics of the weld joint layers

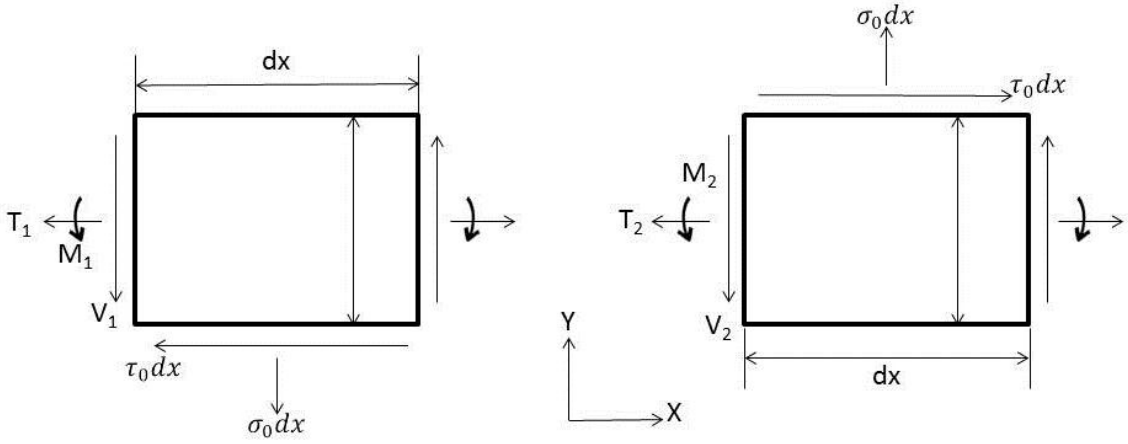

Figure A.2 Moment and force diagrams on the section dx

Equilibrium of moments requires that

$$\frac{dM_1}{dx} - V_1 + \tau_0 \frac{t_1}{2} w_1 = 0 \quad \text{(A.1)}$$

$$\frac{dM_2}{dx} - V_2 + \tau_0 \frac{t_2}{2} w_2 = 0 \quad \text{(A.2)}$$

Equilibrium of forces in X and Y directions requires that

X – direction:

$$\frac{dF_1}{dx} - \tau_0 w_1 = 0 \quad \text{(A.3)}$$

$$\frac{dF_2}{dx} + \tau_0 w_2 = 0 \quad \text{(A.4)}$$

Y – direction:

$$\frac{dV_1}{dx} - \sigma_0 w_1 = 0 \quad \text{(A.5)}$$

$$\frac{dV_2}{dx} + \sigma_0 w_2 = 0 \quad \text{(A.6)}$$

From elementary bending theories,

$$\frac{d^2V_1}{dx^2} = -\frac{M_1}{D_1} \quad \text{(A.7)}$$

where $D_1 = \frac{E_1 t_1^3}{12(1-\gamma_1^2)}$

$$\frac{d^2V_2}{dx^2} = -\frac{M_2}{D_2} \quad \text{(A.8)}$$

where $D_2 = \frac{E_2 t_2^3}{12(1-\gamma_2^2)}$

By assuming linear thermal expansion with constant thermal expansion coefficient,

$$\frac{du_1}{dx} = \frac{(1-\gamma_1^2)F_1}{E_1 t_1 w_1} - \frac{6(1-\gamma_1^2)M_1}{E_1 t_1^2 w_1} + (1+\gamma_1)\alpha_1 T \quad \text{(A.9)}$$

$$\frac{du_2}{dx} = \frac{(1-\gamma_2^2)F_2}{E_2 t_2 w_2} + \frac{6(1-\gamma_2^2)M_2}{E_2 t_2^2 w_2} + (1+\gamma_2)\alpha_2 T \quad \text{(A.10)}$$

where at the Interface:

$$\tau_0 = \frac{G_1 \mu_1}{t_1} - \frac{G_2 \mu_2}{t_2} \quad \text{(A.11)}$$

$$\sigma_0 = \frac{E_1 v_1}{t_1} - \frac{E_2 v_2}{t_2} \qquad \text{(A.12)}$$

Now the stress analysis problem becomes twelve fully formulated differential equations. With appropriate initial and boundary conditions, a solution of these equations can be found numerically for the temperature change from -40 ^{o}C to 90 ^{o}C and the shear stress plot at the interface was shown in Figure A.3 with the maximum shear stress as 13.9 MPa at the free edge of the two bonded joints and this is equivalent to an externally applied force of 27.7 N, which is much less than the endurance limit (110 N) of the joint.

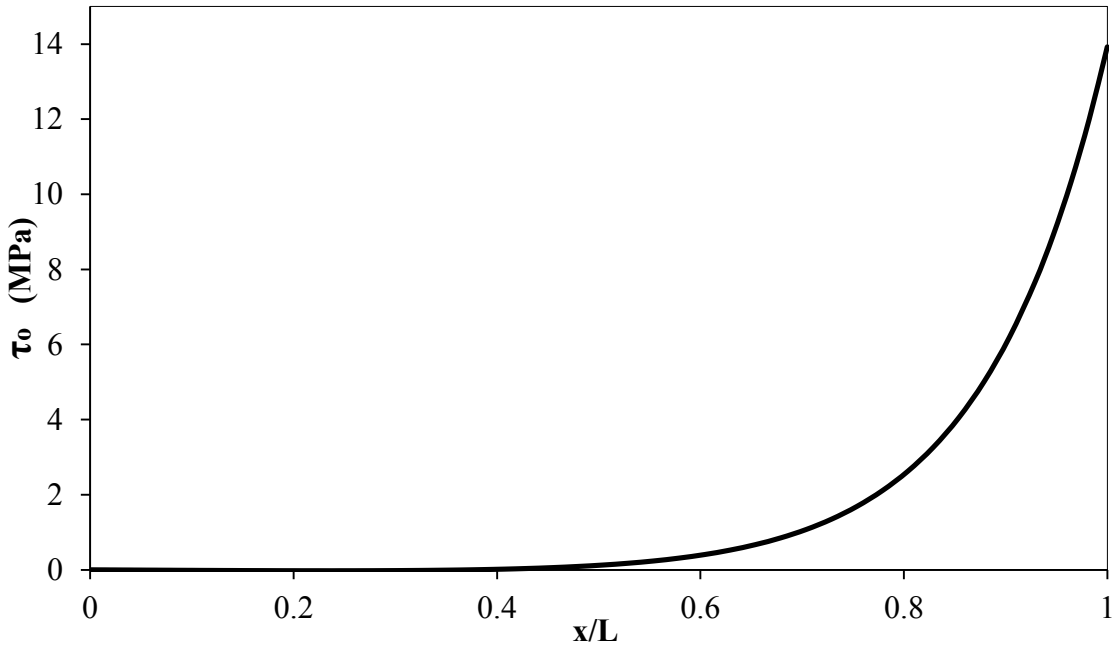

Figure A.3 Linear shear stress distribution at the interface between aluminum and copper

References

1. Sandy Thomas, C., *Transportation options in a carbon-constrained world: Hybrids, plug-in hybrids, biofuels, fuel cell electric vehicles, and battery electric vehicles.* International Journal of Hydrogen Energy, 2009. **34**(23): p. 9279-9296.
2. Eom, S.W., et al., *Life prediction and reliability assessment of lithium secondary batteries.* Journal of Power Sources, 2007. **174**(2): p. 954-958.
3. Meissner, E. and G. Richter, *The challenge to the automotive battery industry: the battery has to become an increasingly integrated component within the vehicle electric power system.* Journal of Power Sources, 2005. **144**(2): p. 438-460.
4. Chan, C., *The state of the art of electric and hybrid vehicles.* Proceedings of the IEEE, 2002. **90**(2): p. 247-275.
5. Neglur, S. and M. Ferdowsi. *Effect of battery capacity on the performance of plug-in hybrid electric vehicles*. in *Vehicle Power and Propulsion Conference, 2009. VPPC'09. IEEE*. 2009. IEEE.
6. Lee, S.S., et al. *Joining Technologies for Automotive Lithium-Ion Battery Manufacturing: A Review*. 2010. ASME.
7. Ponnappan, R. and T. Ravigururajan, *Contact thermal resistance of Li-ion cell electrode stack.* Journal of Power Sources, 2004. **129**(1): p. 7-13.
8. Coffin, J., U.S.A.E. Commission, and G.E. Company, *A Study of the Effects of Cyclic Thermal Stresses on a Ductile Metal*1953: Knolls Atomic Power Laboratory.
9. Manson, S.S. and U.S.N.A.C.f. Aeronautics, *Behavior of Materials Under Conditions of Thermal Stress*1953: National Advisory Committee for Aeronautics.
10. Alves, M., J. Yu, and N. Jones, *On the elastic modulus degradation in continuum damage mechanics.* Computers & Structures, 2000. **76**(6): p. 703-712.
11. Fargione, G., et al., *Rapid determination of the fatigue curve by the thermographic method.* International Journal of Fatigue, 2002. **24**(1): p. 11-19.
12. Fatemi, A. and L. Yang, *Cumulative fatigue damage and life prediction theories: a survey of the state of the art for homogeneous materials.* International Journal of Fatigue, 1998. **20**(1): p. 9-34.
13. Lemaitre, J. and J. Dufailly, *Damage measurements.* Engineering Fracture Mechanics, 1987. **28**(5): p. 643-661.
14. Yang, L. and A. Fatemi, *Cumulative fatigue damage mechanisms and quantifying parameters: a literature review.* Journal of testing and evaluation, 1998. **26**(2): p. 89-100.
15. Chung, D., *Structural health monitoring by electrical resistance measurement.* Smart materials and structures, 2001. **10**(4): p. 624.
16. Constable, J.H. and C. Sahay, *Electrical resistance as an indicator of fatigue.* Components, Hybrids, and Manufacturing Technology, IEEE Transactions on, 1992. **15**(6): p. 1138-1145.

17. Charrier, J. and R. Roux, *Evolution of damage fatigue by electrical measure on smooth cylindrical specimens.* Nondestructive Testing And Evaluation, 1991. **6**(2): p. 113-124.
18. Sun, B. and Y. Guo, *High-cycle fatigue damage measurement based on electrical resistance change considering variable electrical resistivity and uneven damage.* International Journal of Fatigue, 2004. **26**(5): p. 457-462.
19. Beauregard, G.P. and A. Phoenix, *Report of investigation: hybrids plus plug in hybrid electric vehicle.* National Rural Electric Cooperative Association, Inc. and US Department of Energy, Idaho National Laboratory by etec, Online im Internet: URL: http://www. evworld. com/library/prius_fire_forensics. pdf [Stand 11.04. 2012], 2008.
20. Society, A.W., *Handbook for Resistance Spot Welding*1998: American Welding Society.
21. Mys, I. and M. Schmidt. *Laser micro welding of copper and aluminum*. in *Lasers and Applications in Science and Engineering*. 2006. International Society for Optics and Photonics.
22. Janaki Ram, G., Y. Yang, and B. Stucker, *Effect of process parameters on bond formation during ultrasonic consolidation of aluminum alloy 3003.* Journal of Manufacturing Systems, 2006. **25**(3): p. 221-238.
23. Yang, Y., G.D.J. Ram, and B.E. Stucker, *An analytical energy model for metal foil deposition in ultrasonic consolidation.* Rapid Prototyping Journal, 2010. **16**(1): p. 20-28.
24. Ahmed, N., *New developments in advanced welding*2005: CRC Press.
25. Grewell, D.A., A. Benatar, and J.B. Park, *Plastics and composites welding handbook*. Vol. 10. 2003: Hanser Gardner Publications.
26. Hetrick, E., et al., *Ultrasonic Metal Welding Process Robustness in Aluminum Automotive Body Construction Applications.* Welding journal, 2009. **88**(7).
27. Ram, G.D.J., et al., *Use of ultrasonic consolidation for fabrication of multi-material structures.* Rapid Prototyping Journal, 2007. **13**(4): p. 226-235.
28. Manson, S.S., *Thermal stress and low-cycle fatigue*1966: McGraw-Hill.
29. Chen, W. and C. Nelson, *Thermal stress in bonded joints.* IBM Journal of Research and Development, 1979. **23**(2): p. 179-188.
30. Darwish, S. and A. Al-Samhan, *Thermal stresses developed in weld-bonded joints.* Journal of materials processing technology, 2004. **153**: p. 971-977.
31. Taylor, T. and F. Yuan, *Thermal stress and fracture in shear-constrained semiconductor device structures.* Electron Devices, IRE Transactions on, 1962. **9**(3): p. 303-308.
32. Starke, P., F. Walther, and D. Eifler, *PHYBAL—A new method for lifetime prediction based on strain, temperature and electrical measurements.* International Journal of Fatigue, 2006. **28**(9): p. 1028-1036.
33. Starke, P., F. Walther, and D. Eifler, *Fatigue assessment and fatigue life calculation of quenched and tempered SAE 4140 steel based on stress–strain*

hysteresis, temperature and electrical resistance measurements. Fatigue & Fracture of Engineering Materials & Structures, 2007. **30**(11): p. 1044-1051.
34. Lemaître, J. and J.-L. Chaboche, *Mechanics of solid materials*1990, Cambridge: Cambridge University Press.
35. Xiao, Y.C., S. Li, and Z. Gao, *A continuum damage mechanics model for high cycle fatigue.* International Journal of Fatigue, 1998. **20**(7): p. 503-508.
36. Chaboche, J., *Continuum damage mechanics. I- General concepts. II- Damage growth, crack initiation, and crack growth.* ASME, Transactions, Journal of Applied Mechanics, 1988. **55**: p. 59-72.
37. Manson, S., *Some useful concepts for the designer in treating cumulative fatigue damage at elevated temperatures.* Mechanical behaviour of materials, 1980: p. 13-45.
38. Marco, S. and W. Starkey, *A concept of fatigue damage.* Trans. ASME, 1954. **76**(4): p. 627-632.
39. Levenberg, K., *A method for the solution of certain problems in least squares.* Quarterly of applied mathematics, 1944. **2**: p. 164-168.
40. Marquardt, D.W., *An algorithm for least-squares estimation of nonlinear parameters.* Journal of the Society for Industrial & Applied Mathematics, 1963. **11**(2): p. 431-441.

Vita

Nanzhu Zhao was born on 31st October 1986 in China. He received the Brigham Young Scholarship to attend Brigham Young University and graduated with a B.S. degree major in Mechanical Engineering and minor in Mathematics in April 2010. He continued to attend the University of Texas at Austin in August 2010 to obtain an M.S. degree in Mechanical Engineering where he has received Cockrell School of Engineering Fellowship for two consecutive years. For research, he has worked on the fatigue analysis of the ultrasonically welded battery joints supported by Dr. Wei Li.

Permanent email: zhaonanzhu@gmail.com

This thesis was typed by Nanzhu Zhao